LAWRENCE
LIVERMORE
NATIONAL
LABORATORY

UCRL-JRNL-224498

Effects of Fe spin transition on the elasticity of (Mg,Fe)O magnesiowüstites and implications for the seismological properties of the Earth's lower mantle

S. Speziale, V. E. Lee, S. M. Clark, J. F. Lin, M. P. Pasternak, R. Jeanloz

September 1, 2006

Journal of Geophysical Research

Disclaimer

Effects of Fe spin transition on the elasticity of (Mg,Fe)O magnesiowüstites and implications for the seismological properties of the Earth's lower mantle

S. Speziale[1#], V.E. Lee[1], S.M. Clark[2], J. F. Lin[3], M.P. Pasternak[4], R. Jeanloz[1]

[1]Department of Earth and Planetary Science, University of California, Berkeley CA 94720 U.S.A.

[2]Advanced Light Source, Lawrence Berkeley National Laboratory, Berkeley, CA 94720, U.S.A.

[3]Lawrence Livermore National Laboratory, 7000 East Avenue, Livermore, CA 94550, U.S.A.

[4]School of Physics and Astronomy, Tel Aviv University, 69978 Tel Aviv, Israel.

[#]Now at GeoForschungsZentrum Potsdam, Telegrafenberg, 9, 14473 Potsdam, Germany

Abstract. High-pressure x-ray diffraction of $(Mg_{0.8}Fe_{0.2})O$ at room temperature reveals a discontinuity in the bulk modulus at 40 (± 5) GPa, similar pressure at which an electronic spin-pairing transition of Fe^{2+} is also observed. In the x-ray diffraction experiments the transition is completed only at 80 GPa, possibly reflecting lack of equilibration. Combining recent measurements, we document anomalies in the compression curve of Mg-rich magnesiowüstites that are manifestations of the spin transition. The best fit to a third order Birch-Murnaghan equation for the low-spin phase of magnesiowüstite with 17-20 mol% FeO yields bulk modulus K_{T0} = 190 (± 150) GPa, pressure derivative $(\partial K_T/\partial P)_{T0}$ = 4.6 (± 2.7) and unit-cell volume V_0 = 71 (± 5) Å^3, consistent with past estimates of the ionic radius of octahedrally-coordinated low-spin Fe^{2+} in oxides. A sharp spin transition at lower-mantle depths between 1100 and 1900 km (40-80 GPa) would cause a unit-cell volume decrease (ΔV) of 3.7 (± 0.8) to 2.0 (± 0.2) percent and bulk sound velocity increase (Δv_ϕ) of 8.1 (± 6-1.7) percent ($v_\phi = \sqrt{K_S/\rho}$). Even in the absence of a visible seismic discontinuity, we expect the Fe-spin transition to imply a correction to current compositional models of the lower mantle, with up to 10 mol percent increase of magnesiowüstite being required to match the seismological data.

Introduction

The behavior of ferrous iron (Fe^{2+}) in the oxide minerals of the Earth's deep interior has long attracted attention because of the importance of this transition element in influencing chemical partitioning and reactions among mantle minerals and with core material, as well as thermal and electrical transport properties and mechanical properties at depth [e.g., Fyfe, 1960; Burns, 1970; Gaffney and Anderson, 1973; Sherman, 1988; Cohen et al., 1998; Lin et al., 2005; Goncharov et al., 2006; Lin et al., 2006]. Mg-rich magnesiowüstite with composition between $(Mg_{0.9}Fe_{0.1})O$ and $(Mg_{0.6}Fe_{0.4})O$ is expected to be the second most abundant mineral of the Earth's lower mantle, after $(Mg,Fe)SiO_3$ perovskite. However, because of its simpler crystal structure and higher Fe content one expects that the properties of magnesiowüstite can be especially sensitive to the electronic properties of iron. Electronic transitions at the conditions of the Earth's deep interior also have the potential to strongly affect the static structure and dynamics, and hence the evolution of our planet.

In recent years, the pressure-induced transition of Fe from high-spin (HS; or spin unpaired) to low-spin (LS; or spin paired) has been experimentally observed in magnesiowüstite by means of several experimental techniques [Pasternak et al., 1997; Badro et al., 1999, 2003; Lin et al., 2005; Speziale et al., 2005; Lin et al., 2006; Kantor et al., 2006]. The picture emerging from recent experimental results is that the pressure at which the HS→LS transition begins increases with increasing FeO content, from 40 - 60 GPa for 10 mol% FeO to > 80 - 90 GPa for Fe-rich compositons and FeO (Fig. 1) [Pasternak et al., 1997, Badro et al., 1999, 2003; Lin et al., 2005, 2006; Speziale et al., 2005]. The overall picture emerging from computational studies is in general agreement with the experimental results [Tsuchiya et al., 2006; Persson et al., 2006].

Both Lin et al. [2005] and Speziale et al. [2005] have independently combined x-ray diffraction measurements with separate determinations of the spin state of Fe in (Mg,Fe)O, by x-

ray emission spectroscopy or Mössbauer spectroscopy, respectively. Here we combine the results of these two studies, and expand on the interpretation of the effects of the spin transition on elastic properties relevant to the Earth's mantle.

Experiment

The data described in this study are the results of room-temperature synchrotron X-ray diffraction measurements on powders of $(Mg_{0.8}Fe_{0.2})O$, $(Mg_{0.1}Fe_{0.9})O$ [Speziale et al., 2005] and $(Mg_{0.83}Fe_{0.17})O$ [Lin et al., 2005] compressed in gasketed diamond-anvil cells. The measurements on $(Mg_{0.8}Fe_{0.2})O$ and $(Mg_{0.1}Fe_{0.9})O$ were performed at beamline 12.2.2 of the Advanced Light Source, Lawrence Berkeley National Laboratory [Kunz et al., 2005], with additional measurements performed at beamline 13ID-D (GeoSoilEnviro CARS) and at 16ID-B (High-Pressure Collaborative Access Team) of the Advanced Photon Source, Argonne National Laboratory; these samples were loaded in methanol – ethanol – water mixture (16:3:1 volume ratio) or argon as pressure transmitting medium and annealed after pressure increase up to 450 K for about 30 minutes. All the measurements of $(Mg_{0.83}Fe_{0.17})O$ were performed at the High-Pressure Collaborative Access Team of the Advanced Photon Source, Argonne National Laboratory; this sample was loaded in neon pressure medium with platinum as pressure calibrant and was not annealed at high pressures. Further experimental details have been given by Speziale et al. [2005] and Lin et al. [2005].

Results and Discussion

We have determined the unit-cell parameters of $(Mg_{0.8}Fe_{0.2})O$ and $(Mg_{0.1}Fe_{0.9})O$ from x-ray diffraction patterns of the two compositions, mixed together, taken up to 62 GPa (Fig. 2). The Fe-rich composition undergoes a spin transition at pressures above 80 GPa [Speziale et al., 2005], and therefore serves as a reference to document unit-cell volume (hence density) anomalies arising from the electronic transition of Fe^{2+} in $(Mg_{0.8}Fe_{0.2})O$. In particular, the (200) *d*-spacing, corresponding to half the cubic unit-cell parameter (*a*), can be tracked as a function of pressure: the difference in *d*-spacing for the two compositions, $\Delta d_{200} = d_{200}[(Mg_{0.10}Fe_{0.90})O] - d_{200}[(Mg_{0.80}Fe_{0.20})O]$, decreases continuously from 0.029 (± 0.001) Å at ambient pressure to 0.012 (± 0.002) Å at 40 GPa and then starts to increase again, reaching 0.027 (± 0.001) Å by 62 GPa [Speziale et al., 2005]. The reversal in the pressure dependence of Δd_{200} occurs at the same pressure, 40 GPa, at which Mössbauer spectroscopy indicates the onset of the HS→LS transition [Speziale et al., 2005].

$(Mg_{0.1}Fe_{0.9})O$

Above 20 GPa, we observe a structural transition of $(Mg_{0.1}Fe_{0.9})O$ from cubic (B1 structure type, space group $Fm\bar{3}m$) to rhombohedral (space group $R\bar{3}m$) (Fig. 2), in good accord with previous observations on Fe-rich magnesiowüstite [Mao et al., 2002; Kondo et al., 2004]. There is no resolvable discontinuity of molar volume across this structural transition, however (Fig. 3a: the *F-f* plot in the inset essentially shows the derivative of the *P–V* plot).

We fit the data for the cubic polymorph to a third-order Eulerian finite-strain (Birch-Murnaghan) equation of state, obtaining $V_0 = 78.8$ (± 0.1) $Å^3$, $K_{T0} = 150$ (± 7) GPa and $K_{T0}' = 3.6$

(± 0.6) for the room-temperature isotherm. Here, V is the unit-cell volume, K_{T0} the isothermal bulk modulus and $K_{T0}' = (\partial K_T/\partial P)_{T0}$ its pressure derivative, with subscript zero indicating ambient conditions. This result is reinforced by a combined third-order Birch-Murnaghan fit of our data together with those of Mao et al. [2002], yielding V_0 = 78.2 (± 0.1) Å^3, K_{T0} = 156 (± 3) GPa and K_{T0}' = 3.6 (± 0.3) for the room-temperature isotherm. We note that the values of V_0 from the fits are 0.7-1.5 (± 0.1) percent smaller than the volume determined before compression, as well as with the available systematics of the magnesiowüstite solid solution series [Jackson et al., 1978; Bonczar and Graham, 1982; Jacobsen et al., 2002], but in very good agreement with the volume that we measured after compression (Table 1). This behavior is consistent with the 0.3-0.8 percent irreversible unit-cell contraction documented for wüstite taken to high pressures [Hazen et al., 1981], and with the dependence on synthesis conditions of the unit-cell volume of quenched wüstite synthesized at high pressures [McCammon and Liu, 1984]. These differences in zero-pressure unit-cell volumes, before and after compression, have been interpreted as indicating non-equilibrium changes in defect structures upon pressure cycling [Jeanloz and Hazen, 1983; Jeanloz and Sato-Sorensen, 1986]. For the fits to the P–V data, the difficulty of obtaining a V_0 value consistent with the available systematics may be due to the existence of a subtle anomaly in the pressure dependence of the bulk modulus of Fe-rich magnesiowüstites at pressures below 10 GPa, a range that is not densely sampled in our dataset. Recent high-pressure ultrasonic measurements on wüstite present evidences for anomalies in the pressure dependence of the elastic constants C_{11} and C_{12} at 4.7 GPa [Kantor et al., 2004], which could be related to magnetoelastic effects associated with precursors to pressure-induced magnetic ordering (Néel temperature T_N = 300 K at P ~ 17 ± 1 GPa; Sumino et al. [1980]; Yagi et al. [1985]).

Our results for the high-pressure rhombohedral phase are also in agreement with those of Mao et al. [2002], which were collected at room temperature from a sample loaded in He but not annealed. Combining the two datasets yields V_0 = 58.4 (± 0.1) Å^3, K_{T0} = 157 (± 2) GPa and K_{T0}' = 4.1 (± 0.1) for the Birch-Murnaghan isotherm. The large difference between the fit values of V_0 for the cubic and rhombohedral phases is due to the fact that the unit-cell of the cubic phase contains four formula units while that of the rhombohedral phase contains three formula units. The ambient-condition fitted values are 11.86 (± 0.02) cm^3/mol and 11.71 (± 0.03) cm^3/mol for the cubic and rhombohedral phases of $(Mg_{0.1}Fe_{0.9})O$, respectively: compatible with zero volume change at the equilibrium transformation pressure (because the elastic properties of the two phases are not expected to be identical, for example due to magnetoelastic effects, there is therefore no reason to expect the derived zero-pressure molar volumes to be identical even if the cubic–rhombohedral transition is continuous or "second-order"). Decompression results in back-transformation of the rhombohedral phase into the cubic phase at a pressure of 17 GPa.

$(Mg_{0.8}Fe_{0.2})O$

In line with previous results on similar compositions [Jacobsen et al., 2005; Lin et al., 2005], our data show that $(Mg_{0.8}Fe_{0.2})O$ remains cubic (B1 structured) to at least 62 GPa (Fig. 2). Recent ambient-temperature experiments suggest that in the presence of non-hydrostatic stresses, $(Mg_{0.80}Fe_{0.20})O$ undergoes a slight rhombohedral structural distortion at pressures around 30 GPa [Kantor et al., 2006]. However, we did not observe this effect, perhaps because of better hydrostatic conditions in our experiments (e.g., due to annealing).

A combined analysis of x-ray diffraction and Mössbauer data identifies the onset of the spin transition at 40 GPa at room temperature [Speziale et al., 2005]. A Birch-Murnaghan fit of the data below this pressure yields V_0 = 76.03 (± 0.09) Å^3, K_{T0} = 158 (± 3) GPa and K_{T0}' = 4.4 (± 0.2) (Fig. 3b). This bulk-modulus value is in acceptable agreement with recent static-compression measurements on Mg-rich magnesiowüstites, such as $(Mg_{0.64}Fe_{0.36})O$ (V_0 = 77.44 ± 0.03 Å^3, K_{T0} = 154 ± 3 GPa and K_{T0}' = 4.0 ± 0.4; van Westrenen et al. [2005]) and $(Mg_{0.73}Fe_{0.27})O$ (V_0 = 77.30 ± 0.09 Å^3, K_{T0} = 153 ± 3 GPa and K_{T0}' = 4.0 ± 0.1; Jacobsen et al. [2005]). Our measurements are also in good agreement with those of Lin et al. [2005] for $(Mg_{0.83}Fe_{0.17})O$, even though their isotherm parameters (V_0 = 76.10 ± 0.07 Å^3, K_{T0} = 160.7 ± 3.7 GPa and K_{T0}' = 3.28 ± 0.21) different significantly from ours because Lin and coauthors fitted the data up to 56 GPa for the high-spin state and above ~75 Gpa for the low-spin state. Despite the consistency of our bulk modulus value with values obtained from other static-compression measurements on Mg-rich magnesiowüstites, the zero-pressure unit-cell volumes are not so reproducible between studies (cf. the unit-cell volumes of $(Mg_{0.73}Fe_{0.27})O$ given by Jacobsen et al. [2002] and Jacobsen et al. [2005]). The elasticity systematics for Mg-rich magnesiowüstites suggests that, for compositions below 40 mol percent FeO, there is no resolvable variation in bulk modulus with composition. The data point to this conclusion even though differences are quoted in the literature between x-ray diffraction results, that suggest a variation of isothermal bulk modulus between 160 (± 2) GPa for MgO and 154 (± 3) GPa for $(Mg_{0.64}Fe_{0.36})O$ [Fei, 1999; Dewaele et al., 2000; van Westrenen et al., 2005], and ultrasonic measurements that show a variation of the isentropic bulk modulus between 160-162.5 (± 3.0- 0.5) GPa for pure MgO and 164-169 (± 3-11) GPa for compositions between $(Mg_{0.63}Fe_{0.27})O$ and $(Mg_{0.6}Fe_{0.4})O$ [Jackson et al., 1978; Jackson and Niesler, 1982; Bonczar and Graham, 1982; Jacobsen et al., 2002] .

Our x-ray diffraction measurements on $(Mg_{0.8}Fe_{0.2})O$ are consistent with Lin et al.'s [2005] data for $(Mg_{0.83}Fe_{0.17})O$ up to the maximum common pressure of 62 GPa (Fig. 4). As a quantitative test of the agreement between the two datasets, we calculated the ratio of the volume discrepancy between data points in the two datasets divided by their combined 1σ uncertainties $\Delta V/\sum\sigma_V = |(V_{\text{Speziale}} - V_{\text{Lin}})/(\sigma_{V_{\text{Speziale}}} + \sigma_{V_{\text{Lin}}})|$, where V is unit-cell volume at a given pressure and σ its standard deviation (we applied an empirical correction factor to take into account the small pressure differences between data points from the two studies). The resulting consistency parameter varies from 0.2 (± 0.2) at pressures below 34 GPa to 0.8 (± 0.7) at 43-62 GPa, showing that the average deviation between the measurements is less than their joint uncertainty. Given this consistency, we combined the two datasets (Table 3) and fixed the starting volume to the value of 76.10 (± 0.07) $Å^3$ reported by Lin et al. [2005]: identical within uncertainties with our measured starting volume, but more consistent with the systematics of V_0 versus composition of magnesiowüstites [Jackson et al., 1978; Jackson and Niesler, 1982; Bonczar and Graham, 1982; Jacobsen et al., 2002]. Our analysis does not include the results of Jacobsen et al. [2005] for $(Mg_{0.73}Fe_{0.27})O$ because the absolute ambient pressure volume for that composition (V_0 = 77.30 ± 0.02 $Å^3$) is not compatible (within mutual uncertainties) with either our values or the values obtained from systematics of V_0 versus composition [e.g. Jacobsen et al., 2002].

The Birch-Murnaghan fit to the combined dataset up to 40 GPa (high-spin phase) yields K_{T0} = 157.5 (± 0.5) GPa and K_{T0}' = 3.92 ± 0.1 (Fig. 4), consistent with the most recent results for Mg-rich magnesiowüstites as discussed above. This value of K_{T0}' is lower than that obtained by fitting only the data for $(Mg_{0.2}Fe_{0.8})O$, and it is difficult to compare with other existing results for Mg-rich magnesiowüstites due to the substantial inconsistency between different techniques and even between different studies performed using the same techniques [e.g. Jackson et al., 1978;

Bonczar and Graham, 1982; Richet et al., 1989; Fei et al., 1992; Jacobsen et al., 2002, 2005; van Westrenen et al., 2005].

In order to determine the effect of the electronic spin-pairing transition on the density and elasticity of Mg-rich magnesowüstite, we need to know the equation of state for the low-spin phase. Studies to date on a range of similar (Mg-rich) magnesiowüstite compositions show that the transition is complete by pressures of 70-80 GPa (Fig. 1) [Badro et al., 2003; Lin et al., 2005; Speziale et al., 2005; Lin et al., 2006]. For this reason, we focus our analysis of the low-spin $(Mg_{1-x}Fe_x)O$ (x = 0.17-0.2) on Lin et al.'s [2005] data (Table 3) because these are the only x-ray diffraction measurements accessing the appropriate pressure range. Following the approach outlined by Jeanloz [1981], we calculate the Eulerian strain referred to the zero-pressure volume of the high-spin phase (V_0^{HS}), $g = 0.5[(V_0^{HS}/V)^{2/3} - 1]$, for both the high- and low-spin phases of $(Mg_{1-x}Fe_x)O$ (x = 0.17-0.2). We then renormalize the pressure as $G = F \cdot g$, where F is the normalized pressure (see inset in Fig. 3a), and examine G versus g. This analysis enhances discontinuities in the compression curve, and because of the normalization of pressure it is free from assumptions of the starting volume for the high-pressure phase (a limitation of the F versus f approach) [Jeanloz, 1981]. The G versus g plot shows a clear discontinuity at 40 GPa, and a region with reduced slope between 40 and 80 GPa followed by a region with higher slope above 80 GPa that we attribute to the low-spin phase (Fig. 5). The changes in compression-behavior at 40 GPa and 80 GPa are clearly evident in the inset, where the residuals with respect to the model isotherm for the high-spin phase are plotted versus pressure.

The compression of the low-spin phase of $(Mg_{1-x}Fe_x)O$ (x = 0.17-0.2) is similar to that of pure MgO (Figs. 4 and 5): the unit-cell volumes agree to within 1 percent over the 80-135 GPa pressure range, in good accord with Fei et al.'s [2005] findings. In detail, however, the bulk

modulus of low-spin $(Mg_{1-x}Fe_x)O$ (x = 0.17-0.2) appears to be ~ 13.9 (± 0.1) percent higher than that of MgO as a function of pressure (Fig. 6), although we cannot entirely rule out that nonhydrostatic conditions jeopardizes this comparison. A second-order polynomial G versus g fit to Lin et al.'s low-spin data (equivalent to a third order Burch-Murnaghan equation of state) yields V_0 = 71 (± 5) Å^3, K_{T0} = 186 (± 150) GPa and $(\partial K_T/\partial P)_{T0}$ = 4.6 (± 2.7). Evidently, the zero-pressure parameters are only weakly constrained due to the relatively small range of Eulerian strain covered by the available data along with the long extrapolation from 80 GPa to ambient pressure. Still, the best-fit value of unit-cell volume at ambient conditions corresponds to a ratio V_0^{LS}/V_0^{HS} = 0.94 (± 0.06), compatible with the value of 0.957 (± 0.005) expected for $(Mg_{1-x}Fe_x)O$ (x = 0.17-0.2) based on the predicted ionic radius of low- versus high-spin Fe^{2+} in octahedral coordination in oxides [Shannon and Prewitt, 1969]. The value of 0.957 is calculated as the ratio of the volume of a $(Mg_{1-x}Fe^{2+}_x)O_6$ (x = 0.17-0.2) octahedron where Fe^{2+} is in low-spin state (V_{Oct}^{LS}) and that where Fe^{2+} is in the high-spin state (V_{Oct}^{HS}), with the assumption that the system MgO–FeO behaves as an ideal solution at low FeO contents (e.g. Jackson et al. [1978]; Jackson and Niesler [1982]; Bonczar and Graham [1982]; Jacobsen et al.[2002]):

$$V_{Oct}^{LS}/V_{Oct}^{HS} = [x(R^{LS}Fe^{2+} + RO^{2-})^3 + (1-x)(RMg^{2+} + RO^{2-})^3] / [x(R^{HS}Fe^{2+} + RO^{2-})^3 + (1-x)(RMg^{2+} + RO^{2-})^3], \quad (1)$$

where $R^{S}El^{Ox}$ is the effective ionic radius of the elemental species El with spin state S, and oxidation state Ox in octahedral coordination

Using the estimated ionic radii from Shannon and Prewitt [1969]: $R^{LS}Fe^{2+}$ = 0.61 Å, $R^{HS}Fe^{2+}$ = 0.78 Å, RMg^{2+} = 0.72 Å, RO^{2-} = 1.40 Å, we obtain $V_{Oct}^{LS}/V_{Oct}^{HS}$ = 0.957 (± 0.005) for the compositional range $(Mg_{1-x}Fe_x)O$ with x = 0.17-0.2.

We have computed Eulerian strain f and normalized stress F for the low-spin phase of $(Mg_{1-x}Fe_x)O$ (x = 0.17-0.2) for thirteen values of zero pressure unit-cell volumes, between 66.97 and 76.10 Å^3 corresponding to V_0^{LS}/V_0^{HS} between 0.88 and 1.0, that cover the 1σ uncertainty in the volume obtained from the G versus g analysis. For each case, we have performed a Birch-Murnaghan fit of the F versus f data to obtain the parameters K_{T0} and $(\partial K_T/\partial P)_{T0}$, of the isothermal equation of state. The trade-off between zero-pressure equation-of-state properties for the low-spin state is evident from analyzing F versus f, which corresponds approximately to the derivative of a P–V plot (Fig. 7, Table 4). The goodness of fit, expressed by the χ^2 parameter, is insensitive to the assumed value for the zero-pressure volume of the low-spin state, V_0^{LS}, ranging between 66.97 and 76.10 Å^3 (equivalent to V_0^{LS}/V_0^{HS} between 0.88 and 1.0). That is, the model equation of state's misfit in pressure over this range of V_0^{LS} is 1.3-1.5 GPa, which is less than half the average uncertainty in the experimental pressures, and there is a large trade-off with model norm expressed as χ^2 (Fig. 8).

To put the trade-off associated with uncertainties in the zero-pressure properties of the low-spin equation of state into perspective, we consider the differences in volume, bulk modulus and bulk sound velocity ($v_\phi = (K_S/\rho)^{1/2}$ where ρ is density) across the spin transition as a function of pressure across the lower mantle (Fig. 9). In our analysis, we use results obtained at ambient temperature, and assume that the difference in bulk sound velocity between the two phases is unaffected by the conversion from isothermal to adiabatic modulus along the appropriate adiabat for the lower mantle. Only thermal annealing of the system can allow us to understand the characteristics of this transition at equilibrium conditions within the lower mantle. It is not clear at present if any of the high-pressure experiments have been adequately equilibrated. In addition, we only consider the change in properties between high- and low-spin "endmember"

phases, without considering that the existence of the low-spin state of Fe^{2+} introduces a new component in the MgO – FeO system [Speziale et al., 2005]. This new component creates possible conditions for partition of HS and LS intermediate compositions [Dubrovinsky et al., 2000], which still have to be thoroughly explored both experimentally and theoretically.

Over the range of models of the low-spin phase (expressed by the zero-pressure volumes considered here, V_0^{LS}/V_0^{HS} = 0.88 to 1.0), the volume decrease ranges from 3.7 (± 0.8) percent at 40 GPa to 2.0 (± 0.2) percent at 80 GPa. The effect of pressure is greater, over this range, than the uncertainty in the zero-pressure volume of the low-spin phase. Similarly, uncertainty in the zero-pressure volume becomes less important as one considers the jump in bulk modulus or bulk sound velocity with increasing pressure: $\Delta K_T/K_T^{HS} \approx 20$ (± 14-4) percent and $\Delta v_\phi / v_\phi^{HS} \approx 8.1$ (± 6-1.7) percent over the pressure range 40-80 GPa. If we assume the value V_0^{LS}/V_0^{HS} = 0.958, as indicated by the ionic-radius systematics [Shannon and Prewitt, 1969], and we perform the comparison at pressure (transition pressure) ranging from 40 to 80 GPa, then we find that $\Delta V/V^{HS}$, $\Delta K_T/K_T^{HS}$ and $\Delta v_\phi / v_\phi^{HS}$ vary from -3.3 to -2.0 percent, 12 to 17 percent and 3.8 to 7.0 percent, respectively (Fig. 9). Assuming that temperature has little effect upon the sharpness of the transition, these results provide bounds for the overall volume (or density) and velocity change resulting from the spin transition of Fe^{2+} in magnesiowüstite at lower-mantle conditions, based on the available experimental results [Speziale et al., 2005; Lin et al., 2005; Kantor et al., 2005; Fei et al., 2005].

As the abundance of magnesiowüstite is expected to be only of the order of 30 percent in the lower mantle, we have to scale the consequence of the spin transition in a consistent manner in order to assess seismologically observable effects. To derive conservative estimates of the influence of the Fe-spin transition on the properties of the lower mantle, here we neglect the

possibility of a high- to low-spin transition in Mg-Fe silicate perovskite (which, due to its more complex structure may be less sensitive to variations in Fe^{2+} ionic size) and predicted temperature effects on the spin transition in magnesiowüstite [Sturhahn et al., 2005; Tsuchiya et al., 2006]. We thus estimate that the overall effect of the transition ranges between 0.6 (± 0.1) percent and 1.1 (± 0.2) percent density increase and between 2.4 (± 0.5) percent and 2.3 (± 1.0) percent bulk sound velocity increase as the transition pressure varies between 40 to 80 GPa. These changes are comparable to the major discontinuities of the upper mantle and transition zone ($\Delta v_\phi \sim 2 - 3.2$ and ~ 3.4 -5.5 percent at the 410 and 660 km for Dziewonski and Anderson's [1981] PREM and for Kennett et al.'s [1995] ak135, respectively), and they could cause visible seismic anomalies if the spin transition takes place over a narrow depth range.

Various thermodynamic arguments suggest that the effect of temperature is to increase and perhaps broaden the spin-transition pressure [Sherman, 1988; Badro et al., 2003; Lin et al., 2005; Hofmeister, 2006; Sturhahn et al., 2005]. However, experimental results obtained from different groups at different temperatures do not show clear evidence for these temperature effects [Badro et al., 2003; Lin et al., 2005; Speziale et al., 2005; Fei et al., 2005], or they even suggest a negative temperature dependence of the spin crossover pressure [Kantor et al., 2005]. In order to assess the effects of the spin transition broadening, we have analyzed two scenarios of HS→LS transition: one taking place between 40 and 80 GPa, the other between 30 and 120 GPa; these correspond, respectively, to the pressure range observed in our Mössbauer and x-ray diffraction experiments, and to the transition range predicted by Sturhahn et al. [2005] based on a mean-field (Bragg-Williams) model for order-disorder transformations in alloys [Williams, 1935] and Tsuchiya et al [2006].

In order to calculate the effect of a progressive transformation we assume that the properties of Mg-rich magnesiowüstite across the transition are averages of those of the low-pressure and of the high-pressure phases weighted by their relative molar fractions. To calculate this we assume a pressure dependence for the fraction of low-spin phase present of

$$^{LS}Fe/(^{HS}Fe + {}^{LS}Fe) = 1- (P_f - P)/(P_f - P_i) \exp[(P - P_i)/(P_f - P_i)] \quad (2)$$

where ^{LS}Fe and ^{HS}Fe represent the molar fractions ($^{LS}Fe + {}^{HS}Fe = 1$) of the two phases of $(Mg_{1-x}Fe_x)O$ (x = 0.17-0.2), and P_i and P_f are the pressures at which the transition begins and is completed, respectively (Fig. 10). Such a form for the pressure dependence of the transformed fraction reproduces the estimates of low-spin Fe^{2+} abundance obtained by Mössbauer spectroscopy [Speziale et al., 2005]. The relative change in unit-cell volume and bulk sound velocity during the progressive spin transition, $100 \cdot x\Delta V/V^{HS}$ and $100 \cdot x\Delta v_\phi/v_\phi^{HS}$ respectively, are analyzed for both the scenarios across the range of starting unit-cell volume ratio $0.88 < V_0^{LS}/V_0^{HS} < 1.0$ (here x is the molar fraction of the low-spin phase of Mg-rich magnesiowüstite and $\Delta V/V^{HS}$ and $\Delta v_\phi/v_\phi^{HS}$ are calculated for the sharp transition as explained above). In the case of a progressive transition, the volume change for Mg-rich magnesiowüstite is weaker at each pressure than we found for the discrete transition at the corresponding pressure (Fig. 11**)**. Only when the transition is complete does the overall change equal that of a sharp transition at the final pressure (80 or 120 GPa in the two scenarios).

We have also calculated the average percent differences in unit-cell volume and bulk sound velocity across a progressive spin transition in Mg-rich magnesiowüstite (i.e., integrated over the depth ranges shown in Fig. 11). In the case of a transition across the pressure range 40-

80 GPa, the average volume decrease $<\Delta V/V^{HS}>$ is 1.2 ± 0.2 percent and is insensitive to the assumed starting volume ratio V_0^{LS}/V_0^{HS} (Fig. 12a), whereas, the average velocity increase $<\Delta v_\phi/v_\phi^{HS}>$ ranges from 6.2 ± 1.6 percent at V_0^{LS}/V_0^{HS} = 0.88 to 2.8 ± 1.6 percent at V_0^{LS}/V_0^{HS} = 1.0 (Fig. 12b). For a broader pressure range of the spin transition, spanning 30-120 GPa, both the average changes in volume $<\Delta V/V^{HS}>$ and bulk sound velocity $<\Delta v_\phi/v_\phi^{HS}>$ are insensitive to the starting volume ratio V_0^{LS}/V_0^{HS}, averaging 0.6 ± 0.2 percent and 4.2 ± 1.5 percent, respectively (Fig. 12). For a model lower-mantle assemblage containing 30 mol percent Mg-rich magnesiowüstite, the average change in bulk sound velocity is 0.8-1.9 (± 0.5) percent in case of the transition between 40 and 80 GPa and 1.3 (± 0.5) percent for a transition between 30 and 120 GPa. These predicted changes are probably smaller than can be currently resolved by deep-mantle global seismology; in contrast, if the spin transition takes place over a small depth (pressure) range, it should be readily observable.

Even though a progressive transition would likely not produce a detectable seismic discontinuity, the corresponding changes in elastic properties of Mg-rich magnesiowüstite would affect the model bulk sound velocity of a typical lower-mantle mineral assemblage. The differences in bulk elastic properties between a pyrolite-like mineralogical model with and without including the effects of the spin transition could be mis-interpreted as being due to changes in bulk composition of temperature at depth. In order to explore these effects, we considered a mineral assemblage consisting of a ternary mixture of 64 mol percent $(Mg_{0.88}Fe_{0.06}Al_{0.12}Si_{0.94})O_3$ perovskite, 31 mol percent $(Mg_{1-x}Fe_x)O$ (x = 0.17-0.2) and 5 mol percent $CaSiO_3$, which is close to an undepleted peridotite [Lee et al., 2004]. We compared the density and bulk sound velocity of this assemblage, assuming either the progressive spin transition across two different pressure ranges (40 – 80 GPa and 30 – 120 GPa) or no transition,

and evaluated results along a pressure-temperature path corresponding to estimated lower-mantle geotherms [Dziewonski and Anderson, 1981; Brown and Shankland, 1981], and along selected isotherms (Figs. 13 and 14).

We performed the calculations assuming $V_0^{LS}/V_0^{HS} = 0.94$, corresponding to our preferred model for Mg-rich magnesiowüstite. The density and bulk modulus for the different phases were calculated using the Birch-Murnaghan formalism and the Debye model for the thermal pressure [e.g. Jackson and Rigden, 1996]. The Debye tempareture (θ_0), Grüneisen parameter (γ_0) and its logarithmic volume derivative (q) for the three minerals were obtained as averages of the two sets used by Lee et al. [2004] (see discussion in Lee et al. [2004]). The bulk modulus and pressure derivative of (Mg,Fe,Al)SiO_3 perovskite were averages of those presented by Lee et al. [2004] and those from Jackson et al. [2004] and Vanpeteghem et al. [2006], respectively (Table 5). The unit-cell volume and the bulk modulus and pressure derivative for $CaSiO_3$ perovskite were averages of those used by Lee et al. [2004] and those by Shim et al. [2000], and the bulk modulus and pressure derivative for magnesiowüstite were those determined in the present study. In our calculations, we neglected the effect of any spin transition on the elastic properties of Mg-silicate perovskite due to the absence of relevant experimental data (this also means that our results are conservative, in that spin effects in the perovskite are likely to enhance the effects we calculate here). The pressure dependence of the molar fraction of low-spin Mg-rich magnesiowüstite is the same used in the above calculations. Finally, we limited our calculations to the lower mantle above the D" region, and did not consider the effects of the transition from Mg-perovskite to post-perovskite phases [Murakami et al., 2004; Shim et al., 2004; Oganov and Ono, 2004]. The parameters used for our calculations are summarized in Table 5.

Assuming that high temperature does not modify the relative change in volume and bulk modulus across the spin transition, we observe that along the pressure-temperature path corresponding to the geotherm calculated by Brown and Shankland [1981] the occurrence of the spin transition in magnesiowüstite causes a difference of bulk modulus $\Delta K_S/K_{S\text{-}PREM} = (K_{S\text{-}Model} - K_{S\text{-}PREM})/K_{S\text{-}PREM}$ between a pyrolite-type mineral assemblage and the PREM reference model of up to 2.8 percent at the maximum pressure of 120 GPa, approximately 2 times larger than is the case in the absence of the spin transition (Fig. 13). The effect of the spin transition on density is less significant: $\Delta\rho/\rho_{\text{-}PREM} = -0.66$, 15% smaller than in the case of absence of spin transition. The difference between models that do and do not include the spin transition are significant with respect to the estimated uncertainties in the elastic moduli and volumes. The relatively large uncertainties in the thermal parameters (γ_0, θ_0, q) are to all the models, so should not affect our conclusions about the significance of the spin transition (Fig. 13).

Based on the available data, we can only provide tentative estimates of the effects of temperature, mineralogical composition and degree of completion of the spin transition on the density and bulk modulus of model lower-mantle assemblages. The effect of temperature is to decrease the bulk modulus of the assemblage, approaching the PREM model, but also to decrease the overall density, below that of the reference Earth model (Fig. 14). Increasing the amount of Mg-rich magnesiowüstite has the advantage of increasing the overall density at the highest pressures, but also of decreasing the bulk modulus (Fig. 15). Finally, as suggested by Sturhahn et al. [2005] and Tsuchiya et al. [2006], a substantial temperature dependence of the spin-transition pressure and broadening of the spin transition beyond the pressure range of the lower mantle would mitigate the very large rise of the bulk modulus of magnesiowüstite of a model mantle assemblage with respect to the reference PREM model (Fig. 13). Thus, with the

simplifying assumption that the thermal parameters of the equation of state of Mg-rich magnesiowüstite are not affected by the spin-transition, we expect that the lowermost part of the lower mantle is either characterized by a very high thermal gradient (more than 80 percent larger than that predicted by Brown and Shankland [1981]) or by depletion of the SiO_2 content (to less than 55 mol percent Mg-perovskite with respect to a pyrolitic compositional model) (Figs. 14-15). Despite the absence of quantitative information on the effect of the spin transition of Fe on the elastic properties of $(Mg,Fe,Al)SiO_3$ perovskite, we infer that the effect of a progressive spin transition across a broad pressure range is likely to require a revision of the thermal, compositional and mineralogical models of the lowermost mantle, toward hotter and more Si-depleted values than the upper part of the mantle.

Conclusions

Based on our results, the Fe spin transition in magnesiowüstite appears to have an impact on the properties of the lower mantle that is comparable to that of the polymorphic transition of $(Mg,Fe,Al)SiO_3$ from perovskite to post-perovskite phase. Experiments documenting a close approach to quasi-equilibrium conditions, and a better understanding of the thermodynamics of the ternary system high-spin FeO – low-spin FeO – MgO are needed to better clarify the details of this electronic transition of Fe at lower mantle conditions.

Acknowledgments. This research was supported by the University of California. We thank E.K. Graham (Pennsylvania State University) for supplying sample material. We acknowledge the use of the facilities of beamline 12.2.2 at the Advanced Light Source, Lawrence Berkeley National Laboratory, and those of the GeoSoilEnviro-Consortium (GSECARS) and the High-Pressure

Collaborative Access Team (HPCAT) at the Advanced Photon Source, Argonne National Laboratory. The Advanced Light Source is supported by the Director, Office of Science, Office of Basic Energy Sciences, Materials Sciences Division, of the U.S. Department of Energy under Contract No. DE-AC03-76SF00098 at Lawrence Berkeley National Laboratory. GSECARS is supported by the NSF, DOE, and the State of Illinois. HPCAT is supported by DOE-BES, DOE-NNSA (CDAC), NSF, DOD-TACOM, and the W.M. Keck Foundation. Use of APS was supported by the U.S. DOE-S, DOE-BES.This research has been supported by the U.S. Department of Energy and the University of California. This work, in collaboration with J.F.L. was performed under the auspices of the U.S. DOE by University of California and LLNL under Contract No. W-7405-Eng-48. J.F.L. is also supported by the Lawrence Livermore Fellowship. S.S. is supported by the Miller Institute for basic Research in Science.

References

Badro, J., V.V. Struzhkin, J. Shu, R.J. Hemley, and H.K. Mao (1999), Magnetism in FeO at megabar pressures from x-ray emission spectroscopy, *Phys. Rev. Lett., 83*, 4101-4104.

Badro, J., G. Fiquet, F. Guyot, J.-P. Rueff, V.V. Struzhkin, G. Vankó, and G. Monaco (2003), Iron partitioning in Earth's mantle: Towards a deep lower mantle discontinuity, *Science, 300*, 789-791.

Bonczar, L.J., and E.K. Graham (1982), The pressure and temperature dependence of the elastic properties of polycrystal magnesiowüstite, *J. Geophys. Res., 87*, 1061-1078.

Brown, J.M., and T.J. Shankland (1981), Thermodynamic parameters in the Earth as determined from seismic profiles, Geophys. J. Royal Astron. Society, 66, 579-596.

Burns, R.G. (1970), *Mineralogical Applications of Crystal Field Theory*, Cambridge University Press, Cambridge UK.

Cohen, R.E., I.I. Mazin, and D.J. Isaak (1997), Magnetic collapse in transition metal oxides at high pressure: Implications for the Earth, *Science, 275*, 654-657.

Dewaele, A., G. Fiquet, D. Andrault, and D. Hausermann (2000), P-V-T equation of state of periclase from synchrotron radiation measurements, *J. Geophys. Res., 105*, 2869-2877.

Dubrovinsky, L.S., I.Y. Kantor, A. Kantor, C.A. McCammon, and W. Crichton (2005), Phase transition in transition metal monoxides: Interplay between structural, magnetic, and electronic properties, *EOS Trans. AGU, 86 (52)*, Fall Meet. Suppl., Abstract MR34A-07.

Dubrovinsky, L.S., N.A. Dubrovinskaya, H. Annersten, E. Hålenius, H. Harryson, F. Tutti, S. Rekhi, and T. LeBihan (2000), Stability of ferropericlase in the lower mantle, *Science, 289*, 430-432.

Dziewonski, A.M., and D.L. Anderson (1981), Preliminary reference Earth model, *Phys. Earth Planet. Inter., 25*, 297-356.

Fei, Y. (1999), Effects of temperature and composition on the bulk modulus of (Mg,Fe)O, *Am. Mineral., 84*, 272-276.

Fei, Y., H.K. Mao, J. Shu, and J. Hu (1992), P-V-T equation of state of magnesiowüstite $(Mg_{0.6}Fe_{0.4})O$, *Phys. Chem. Minerals, 18*, 416-422.

Fei, Y., L. Zhang, A. Corgne, H.C. Watson, G. Shen, and V.B. Prakapenka (2005), Spin transition in (Mg,Fe)O at high pressure, *EOS Trans. AGU, 86 (52)*, Fall Meet. Suppl., Abstract MR14A-05.

Fyfe, W.S. (1960), The possibility of d-electron coupling in olivine at high pressure, *Geochim. Cosmochim. Acta, 19*, 141-143.

Gaffney, E.S., and D.L. Anderson (1973), Effect of low-spin Fe^{2+} on the composition of the lower mantle, *J. Geophys. Res., 78*, 7005-7014.

Goncharov, A. F., V. V. Struzhkin, and S. D. Jacobsen (2006), Reduced radiative conductivity of low-spin (Mg, Fe)O in the lower mantle, *Science*, *312*, 1205- .

Hammersley, A.P. (1998), FIT2D: V99129 Reference Manual Version 3.1, *Internal Report ESRF-98-HA01*, ESRF, Grenoble, France.

Hazen, R.M., H.K. Mao, L.W. Finger, and P.M. Bell, (1981) Irreversible unit-cell volume changes of wüstite single crystals quenched from high pressure, *Year Book Carnegie Inst. Washington, 80*, 274-277.

Hofmeister, A.M. (2006) Is low-spin Fe^{2+} present in Earth's mantle? *Earth Planet. Sci. Lett., 243*, 44-52.

Kantor, I.Y., L.S. Dubrovinsky, and C.A. McCammon (2005), Spin transition in ferropericlase at high pressures and temperatures: Mössbauer spectroscopic study, *EOS Trans. AGU, 86 (52)*, Fall Meet. Suppl., Abstract MR23A-0038.

Kantor, I.Y., L.S. Dubrovinsky, C.A. McCammon, A. Kantor, S. Pascarelli, G. Aquilanti, W. Crichton, M. Mattesini, R. Ahuja, J. Almeida, and V. Ursov (2006), Pressure-induced phase transition in $Mg_{0.8}Fe_{0.2}O$ ferropericlase, *Phys. Chem. Minerals*, DOI 10.1007/ss00269-005-0052-z.

Kantor, I.Yu., L.S. Dubrovinsky, and C.A. McCammon, Spin crossover in „Mg,Fe…O: A Mössbauer effect study with an alternative interpretation of x-ray emission spectroscopy data, Phys. Rev. B 73, 100101 (2006).

Kennett, B.L.N., E.R. Engdahl, and R. Buland (1995), Constraints on seismic velocities in the Earth from travel times, *Geophys. J. Int., 122*, 108-124.

Kondo, T., E. Ohtani, N. Hirao, T. Yagi, T. Kikegawa (2004), Phase transition of (Mg,Fe)O at high pressures, Phys. Earth Planet. Inter., 143-144, 201-213.

Kunz, M., AA MacDowell, W.A. Caldwell, D. Cambie, R.S. Celestre, E.E. Domning, R.M. Duarte, A.E. Gleason, J.M. Glossinger, N. Kelez, D.W. Plate, T. Yu, J.M. Zaug, H.A. Padmore, R. Jeanloz, A.P. Alivizatos, and S.M. Clark (2005), A beamline for high pressure studies at the Advanced Light Source with a superconducting bending magnet as the source, *J. Synch. Rad*. **12** 650-58.

Jacobsen, S.D., H.-J. Reichmann, H.A. Spetzler, S.J. Mackwell, J.R. Smyth, R.J. Angel, and C.A. McCammon (2002) Structure and elasticity of single-crystal (Mg,Fe)O and a new method of generating shear waves for gigahertz ultrasonic interferometry, J. Geophys. Res., 107, doi:10.1029/2001JB000490, 2002.

Jacobsen, S.D., J.-F. Lin, R.J. Angel, G. Shen, V.B. Prakapenka, P. Dera, H.K. Mao, and R.J. Hemley (2005), Single-crystal synchrotron x-ray diffraction study of wüstite and magnesiowüstite at lower mantle pressures, *J. Synchrotron Rad., 12*, 577-583.

Jackson, I. (1998), Elasticity, composition and temperature of the Earth's lower mantle: a reappraisal, Geophys. J. Int., 134, 291-311.

Jackson I., R.C. Liebermann, and A.E. Ringwood (1978), The elastic properties of (MgxFe1-x)O solid solutions, *Phys. Chem. Miner., 3*, 11-31.

Jackson, I., and S.M. Rigden (1996), Analysis of P – V – T data: constraints on the thermoelastic properties of high-pressure minerals, Phys. Earth Planet. Inter., 96, 85-112.

Jackson, I., and H. Niesler (1982), The elasticity of periclase to 3 GPa and some geophysical implications, in *High Pressure Research in Geophysics*, edited by S.-I. Akimoto and M. manghnani, pp. 93-114, Cent. For Acad. Publish.of Jp., Tokyo.

Jackson, J.M., J. Zhang, and J.D. Bass, Sound velocity and elasticity of aluminous $MgSiO_3$ perovskite: Implications for aluminum heterogeneityin Earth's lower mantle (2004), Geophys. Res. Lett., 31, L10614, doi:10.1029/2004GL019918.

Jeanloz, R. (1981), Finite-strain equation of state for high-pressure phases, *Geophys. Res. Lett., 8*, 1219-1222.

Jeanloz, R., and R.M. Hazen (1983), Compression, nonstoichiometry and bulk viscosity of wüstite, *Nature, 304*, 620-622.

Jeanloz, R., and Y. Sato-Sorensen (1986), Hydrostatic compression of $Fe_{1-x}O$ wüstite, *J. Geophys. Res., 91*, 4665-4672.

LeBail, A. (1992), Extracting structure factors from powder diffraction data by iterating full pattern profile fitting, in *Accuracy in Powder Diffraction II*, edited by E. Prince and J.K Taliek, Special Publication 846, 213, National Bureau of Standards, Gaithersburg, MD.

Lee, K.M., B. O'Neill, W.R. Panero, S.-H. Shim, L.R. Benedetti, and R. Jeanloz (2004), Equations of state of the high-pressure phases of a natural peridotite and implications for the Earth's lower mantle, *Earth Planet. Sci. Lett., 223*, 381-393.

Lin, J.-F., V.V. Struzhkin, S.D. Jacobsen, M.Y. Hu, P. Chow, J. Kung, H. Liu, H.K. Mao, and R.J. Hemley (2005), Spin transition of iron in magnesiowüstite in the Earth's lower mantle, *Nature, 436*, 377-380.

Lin, J.-F., A.G. Gavriliuk, V.V. Struzhkin, S.D. Jacobsen, W. Sturhahn, M.J. Hu, P. Chow, and C.-S. Yoo (2006), Pressure-induced spin transition of iron in magnesiowüstite-(Mg,Fe)O, Phys. Rev. B, 73, 113107, doi:10.1103/PhysRevB.73.113107.

Mao, W., J. Shu, R.J. Hemley, and H.K. Mao (2002), Displacive transition in magnesiowüstite, *J. Phys. Condens. Matter, 14*, 11349-11354.

Mao, H.K., J. Xu, and P.M. Bell (1986), Calibration of the ruby pressure scale to 800 kbar under quasi-hydrostatic conditions, *J. Geophys. Res., 91*, 4673-4677.

McCammon, C.A., and L.G. Liu (1984), The effects of pressure and temperature on nonstoichiometric wüstite, Fe_xO: The iron-rich phase boundary, *Phys. Chem. Miner., 10*, 106-113.

Murakami, M., K. Hirose, K. Kawamura, N. Sata, and Y. Ohishi (2004), Post-perovskite phase transition in $MgSiO_3$, *Science, 304*, 855-858.

Oganov A.R., and S. Ono (2004), Theoretical and experimental evidence for a post-perovskite phase of $MgSiO_3$ in Earth's D" layer, *Nature, 430*, 445-448.

Pasternak, M.P., R.D. Taylor, R. Jeanloz, X. Li, J.H. Nguyen, and C.A. McCammon (1997), High pressure collapse of magnetism in $Fe_{0.94}O$: Mössbauer spectroscopy beyond 100 GPa, *Phys. Rev. Lett., 79*, 5046-5049.

Persson, K, A. Bengtson, G. Ceder, and D. Morgan (2006), Ab initio study of the composition dependence of the pressure-induced spin transitionin the $(Mg_{1-x}Fe_x)O$ system, Geophys. Res. Lett., 33, L16306, doi:10.1029/2006GL026621, 2006.

Piermarini, G.J, S. Block, J.D. Barnett, and R.A. Forman (1975), Calibration of the pressure dependence of the R1 ruby fluorescence line to 195 kbar, *J. Appl. Phys., 46*, 2777-2780.

Richet, P., H.K. Mao, and P.M. Bell (1989), Bulk moduli of magnesiowüstites from static compression measurements, *J. Geophys. Res., 94*, 3037-3045.

Shannon, R.D., and C.T. Prewitt (1969), Effective ionic radii in oxides and fluorides, *Acta Crystallogr., B 25*, 925-946.

Speziale, S., A. Milner, V.E. Lee, S.M. Clark, M.P. Pasternak, and R. Jeanloz (2005), Iron spin transition in Earth's mantle, *Proc. Natl. Acad. Sci. USA, 102*, 17918-17922.

Speziale, S., C.-S. Zha, T.S. Duffy, R.J. Hemley and H.K. Mao (2001), Quasi-hydrostatic compression of magnesium oxide to 52 GPa: Implications for the pressure-volume-temperature equation of state, *J. Geophys. Res., 106*, 515-528.

Sherman, D.M. (1988), High-spin to low-spin transition of iron(II) oxides at high pressures: Possible effects on the physics and chemistry of the lower mantle, in *Structural and Magnetic Phase Transitions in Minerals*, edited by S.Ghose, J.M.D. Coey, and E. Salje, 113-128, Springer-Verlag, New York.

Shim, S.-H., T.S. Duffy, and G. Shen (2000), The equation of state of CaSiO3 perovskite to 108 GPa at 300 K, Phys. Earth and Planet. Inter., 120, 327-338.

Shim, S.-H., T.S. Duffy, R. Jeanloz, and G. Shen (2004), Stability and crystal structure of $MgSiO_3$ perovskite to the core-mantle boundary, *Geophys. Res. Lett., 31*, L10603, doi:10.1029/2004GL019639.

Sturhahn, W., J.M. Jackson, and J.-F. Lin (2005), The spin state of iron in minerals of Earth's lower mantle, *Geophys. Res. Lett., 32*, doi:10.1029/2005GL022802, 2005.

Sumino, Y., M. Kumazawa, O. Nishizawa, and W. Pluschkell (1980), The elastic constants of single-crystal Fe1-xO, MnO and CoO, and the elasticity of stoichiometric magnesiowüstite, *J. Phys. Earth, 28*, 475-495.

Tsuchiya, T., R.M. Wentzcovitch, C.R.S. da Silva, and S. de Gironcoli (2006), Spin transition in magnesiowüstite in Earth's lower mantle, *Phys. Rev. Lett., 96*, 198501.

Vanpeteghem, C.B., J. Zhao, R.J. Angel, N.L. Ross, and N. Bolfan-Casanova (2006), Crystal structure and equation of state of MgSiO3 perovskite, Geophys. Res. Lett., 33, L03306, doi:10.1029/2005GL024955.

van Westrenen, W., J. Li, Y. Fei, MR. Frank, H. Hellwig, T. Komabayashi, K Mibe, W.G. Minarik, J.A. Van Orman, H.C. Watson, K.-I. Funakoshi, and M.W. Schmidt (2005), Thermoelastic properties of $(Mg_{0.64}Fe_{0.46})O$ ferropericlase based on in situ X-ray diffraction to 26.7 GPa and 2173 K, *Phys. Earth Planet. Inter., 151*, 163-176.

Williams, E.J. (1935), The effect of thermal agitation on atomic arrangement in alloys III, *Proc. R. Soc. London, Ser. A, 152*, 231-252.

Yagi, T., T. Suzuki, and S.-I. Akimoto (1985), Static compression of wüstite to 120 GPa, *J. Geophys. Res., 90*, 8784-8788.

Table 1a. Unit-cell volume and molar volume of $(Mg_{0.1}Fe_{0.9})O$ (B1 phase) at high pressure

Pressure (GPa)	V ($Å^3$)	V (cm^3/mol)	Experimental details
10^{-4}	79.37 ± 0.39	11.95 ± 0.08	
10^{-4}	78.84 ± 0.26	11.87 ± 0.05	decompression
0.5 ± 0.2	78.37 ± 0.60	11.80 ± 0.12	decompression
4.0 ± 0.2	75.90 ± 0.42	11.43 ± 0.08	decompression
10.8 ± 0.1	73.66 ± 0.65	11.09 ± 0.02	decompression
13.0 ± 1	72.65 ± 0.47	10.94 ± 0.09	decompression
13.3 ± 0.7	72.20 ± 0.57	10.87 ± 0.11	decompression
13.8 ± 0.4	72.36 ± 0.68	10.89 ± 0.14	compression
15.0 ± 2	72.00 ± 0.37	10.84 ± 0.07	compression
17.0 ± 0.5	71.56 ± 0.48	10.77 ± 0.10	decompression
19.0 ± 2	70.70 ± 0.51	10.64 ± 0.10	compression
21.0 ± 1	70.24 ± 0.53	10.57 ± 0.11	compression
25.0 ± 2	69.86 ± 0.95	10.52 ± 0.19	compression
30.0 ± 1	68.09 ± 0.70	10.25 ± 0.14	compression
31.1 ± 0.6	67.65 ± 0.70	10.18 ± 0.14	compression

Table 1b. Unit-cell volume and molar volume of $(Mg_{0.1}Fe_{0.9})O$ (rhombohedral phase) at high pressure

Pressure (GPa)	V ($Å^3$)	V (cm^3/mol)	Experimental details
25.0 ± 2	50.77 ± 0.95	10.19 ± 0.19	compression
27.8 ± 0.5	51.23 ± 0.75	10.28 ± 0.15	compression
30.0 ± 1	50.73 ± 0.91	10.18 ± 0.18	compression
31.1 ± 0.6	50.81 ± 0.37	10.20 ± 0.07	compression
33.9 ± 0.6	49.91 ± 0.90	10.02 ± 0.18	compression
36.0 ± 1	49.70 ± 0.94	9.98 ± 0.19	compression
38.4 ± 0.5	49.50 ± 0.94	9.93 ± 0.19	compression
39.5 ± 0.1	49.33 ± 0.79	9.90 ± 0.16	compression
42.1 ± 0.4	48.72 ± 0.63	9.78 ± 0.13	decompression
43.0 ± 3	48.90 ± 0.83	9.82 ± 0.17	compression
44.7 ± 0.9	48.65 ± 0.49	9.77 ± 0.10	decompression
44.7 ± 0.8	48.74 ± 0.70	9.78 ± 0.14	decompression
47.0 ± 3	47.40 ± 0.80	9.51 ± 0.16	compression
52.0 ± 3	47.22 ± 0.49	9.48 ± 0.10	compression
52.0 ± 3	46.85 ± 0.80	9.40 ± 0.16	compression
54.0 ± 2	47.21 ± 0.37	9.48 ± 0.07	compression
55.0 ± 3	47.37 ± 0.42	9.51 ± 0.08	compression
57.0 ± 3	46.42 ± 0.79	9.32 ± 0.16	compression
62.0 ± 2	45.99 ± 0.70	9.23 ± 0.14	compression
62.0 ± 2	46.34 ± 0.37	9.30 ± 0.07	compression

Table 2. Unit cell volume of $(Mg_{0.8}Fe_{0.2})O$ at high pressure

Pressure (GPa)	V ($Å^3$)	Experimental details
10^{-4}	76.30 ± 0.25	
0.5 ± 0.2	75.93 ± 0.95	decompression
10.8 ± 0.1	71.39 ± 0.92	decompression
13.0 ± 1	70.24 ± 0.70	decompression
13.3 ± 0.7	70.00 ± 0.80	decompression
13.8 ± 0.4	69.85 ± 0.78	compression
15.0 ± 2	70.00 ± 0.59	compression
17.0 ± 0.5	69.34 ± 0.35	decompression
19.0 ± 2	68.70 ± 0.43	compression
21.0 ± 1	68.11 ± 0.35	compression
25.0 ± 2	67.12 ± 0.37	compression
27.8 ± 0.5	66.61 ± 0.36	compression
30.0 ± 1	66.41 ± 0.32	compression
31.1 ± 0.6	66.41 ± 0.30	compression
33.9 ± 0.6	65.29 ± 0.27	compression
36.0 ± 1	64.55 ± 0.27	compression
38.4 ± 0.5	64.46 ± 0.27	compression
39.5 ± 0.1	64.08 ± 0.21	compression
42.1 ± 0.4	63.30 ± 0.34	decompression
43.0 ± 3	63.20 ± 0.27	compression
44.7 ± 0.9	62.99 ± 0.36	decompression
44.7 ± 0.8	63.13 ± 0.27	decompression
47.0 ± 3	61.89 ± 0.41	compression
52.0 ± 3	61.16 ± 0.41	compression
52.0 ± 3	60.85 ± 0.26	compression
54.0 ± 2	61.15 ± 0.31	compression
55.0 ± 3	61.12 ± 0.33	compression
57.0 ± 3	59.78 ± 0.41	compression
62.0 ± 2	58.61 ± 0.36	compression
62.0 ± 2	59.13 ± 0.31	compression

Table 3. Unit cell volume of $(Mg_{0.83}Fe_{0.17})O$ at high pressure*

Pressure (GPa)	V ($Å^3$)	Experimental details
10^{-4}	76.10 ± 0.07	
1.0 ± 0.1	75.60 ± 0.02	compression
8.0 ± 0.5	72.78 ± 0.08	compression
9.6 ± 0.5	72.25 ± 0.22	compression
10.3 ± 0.6	71.66 ± 0.12	compression
10.8 ± 1.2	71.22 ± 0.23	compression
13.2 ± 0.7	70.42 ± 0.17	compression
14.4 ± 1.2	69.95 ± 0.23	compression
16.0 ± 0.8	69.58 ± 0.22	compression
18.5 ± 0.4	68.86 ± 0.25	compression
20.9 ± 0.6	68.23 ± 0.28	compression
27.5 ± 0.8	66.53 ± 0.29	compression
29.6 ± 0.9	66.00 ± 0.34	compression
31.4 ± 0.9	65.79 ± 0.33	compression
33.9 ± 1.4	64.94 ± 0.15	compression
43.1 ± 1.3	62.83 ± 0.23	compression
43.4 ± 1.3	62.96 ± 0.15	compression
45.3 ± 1.4	62.26 ± 0.21	compression
47.2 ± 1.4	61.81 ± 0.23	compression
50.1 ± 1.5	61.01 ± 0.23	compression
50.3 ± 1.5	60.63 ± 0.23	compression
50.9 ± 1.5	60.55 ± 0.23	compression
55.1 ± 1.7	59.94 ± 0.28	compression
59.2 ± 1.8	58.80 ± 0.27	compression
61.8 ± 1.9	58.29 ± 0.27	compression
63.7 ± 1.9	58.20 ± 0.27	compression
65.4 ± 3.4	57.76 ± 0.27	compression
70.2 ± 2.1	57.35 ± 0.27	compression
73.6 ± 2.2	56.87 ± 0.22	compression
74.3 ± 2.2	56.20 ± 0.24	compression
74.8 ± 2.2	56.85 ± 0.24	compression
76.4 ± 2.3	56.15 ± 0.26	compression
80.9 ± 2.8	55.89 ± 0.29	compression
83.5 ± 2.5	55.55 ± 0.24	compression
85.3 ± 3.4	55.22 ± 0.22	compression
87.7 ± 2.6	55.04 ± 0.22	compression
89.6 ± 2.7	54.87 ± 0.26	compression
91.3 ± 2.7	54.78 ± 0.24	compression
94.5 ± 2.8	54.50 ± 0.26	compression
95.7 ± 2.9	54.24 ± 0.26	compression

98.4 ± 3	54.01 ± 0.24	compression
100.8 ± 3	53.86 ± 0.21	compression
103.9 ± 3.1	53.66 ± 0.23	compression
104.5 ± 3.1	53.49 ± 0.30	compression
109.9 ± 3.3	53.18 ± 0.27	compression
115.0 ± 3.5	52.55 ± 0.21	compression
125.4 ± 3.8	51.80 ± 0.29	compression
126.5 ± 4.7	51.59 ± 0.20	compression
134.1 ± 6.7	51.41 ± 0.29	compression

*Experimental details are reported in Lin et al. [2005].

Table 4. Fit parameters of the 3rd order Birch – Murnaghan isotherm of the low-spin phase of $(Mg_{0.8}Fe_{0.2})O$ for various initial ratios V_0^{LS}/V_0^{HS}

V_0^{LS}/V_0^{HS}	K_0 (GPa)	K_0'	χ^2	RMS misfit (GPa)
0.88	339 ± 28	3.0 ± 0.7	0.782	1.55
0.89	304 ± 27	3.3 ± 0.7	0.780	1.49
0.90	273 ± 26	3.6 ± 0.7	0.784	1.45
0.91	246 ± 25	3.9 ± 0.7	0.793	1.41
0.92	222 ± 24	4.1 ± 0.8	0.804	1.39
0.93	200 ± 23	4.4 ± 0.8	0.817	1.37
0.94	182 ± 22	4.7 ± 0.8	0.831	1.36
0.95	165 ± 22	4.9 ± 0.8	0.845	1.35
0.96	149 ± 21	5.2 ± 0.8	0.858	1.34
0.97	136 ± 20	5.4 ± 0.9	0.872	1.34
0.98	123 ± 20	5.7 ± 0.9	0.884	1.33
0.99	112 ± 19	6.0 ± 0.9	0.897	1.33
1.00	101 ± 19	6.2 ± 0.9	0.908	1.32

Table 5. Parameters of the 3rd order Birch–Murnaghan equation of state and Debye model for $(Mg_{0.89}Fe_{0.11})SiO_3$, the low-spin and high-spin phases of $(Mg_{0.83}Fe_{0.17})O$

Par.	$(Mg_{0.88}Fe_{0.06}Al_{0.12}Si_{0.94})O_3$	$(Mg_{0.83}Fe_{0.17})O$ (HS)	$(Mg_{0.83}Fe_{0.17})O$ (LS)	$CaSiO_3$
V_0 (Å^3)	163.9[a]	76.10[d]	71.39[d]	45.37 ± 0.1[e]
Mol. wt. (g)	102.38	45.67	45.67	116.17 ± e
K_{T0} (GPa)	260 ± 10[b]	157.5 ± 0.5[d]	186 ± 22[d]	259 ± 20[e]
$(\partial K_T/\partial P)_{T0}$	4.03 ± 0.03[c]	3.92 ± 0.1[d]	4.6 ± 0.8[d]	3.9 ± 0.1[e]
θ_0 (K)	1009 ± 9[a]	587 ± 80[a]	587 ± 80[a]	1100[a]
γ_0	1.64 ± 0.3[a]	1.46 ± 0.05[a]	1.46 ± 0.05[a]	1.7[a]
q	1.75 ± 0.7[a]	1.2 ± 0.1[a]	1.2 ± 0.1[a]	1[a]

The uncertainties reported in this table are estimated ranges of variation between the available literature data.
[a]Lee et al. [2004] – average of high- and low-thermal expansion set of parameters (see Lee et al. [2004] for details).
[b]Average of Lee et al. [2004] and Jackson et al. [2004].
[c]Average of Lee et al. [2004] and Vanpeteghem et al. [2006].
[d]This study.
[e]Average of Shim et al. [2000] and lee et al. [2004].

Figure Captions

Figure 1. Phase diagram indicating the electron-spin transition of Fe^{2+} in magnesiowüstite as a function of pressure and composition: open and closed symbols indicate high- and low-spin states, respectively, and grey symbols indicate coexisting spin states (data from Pasternak et al. [1997]; Badro et al. [1998, 2003]; Lin et al. [2005, 2006]; Speziale et al. [2005]; and, for $Mg_{0.90}Fe_{0.10}O$, from unpublished work of Pasternak). Lines indicate onset and completion of the high- to low-spin transition.

Figure 2. X-ray powder diffraction patterns of $(Mg_{0.8}Fe_{0.2})O$ + $(Mg_{0.1}Fe_{0.9})O$ (3:1 volume ratio), and integrated intensities vs. scattering angle (2θ) refined with the full-pattern fitting method: (a) Image and (b) integrated pattern before the structural transition of $(Mg_{0.1}Fe_{0.9})O$; (c) Image and (d) integrated pattern after the cubic to rhombohedral transition of $(Mg_{0.1}Fe_{0.9})O$.

Figure 3. Isothermal compression curves of $(Mg_{0.8}Fe_{0.2})O$ and $(Mg_{0.1}Fe_{0.9})O$ between 0 and 62 GPa at 300 K. (a) Pressure–volume (*P*–*V*) data for cubic and rhombohedral phases of $(Mg_{0.1}Fe_{0.9})O$, and corresponding third-order Eulerian finite-strain (Birch–Murnaghan) equation of state (curve, dashed outside stability pressure range), and (*inset*) the same dataset plotted in terms of normalized pressure ($F = P/[3f(1+2f)^{5/2}]$) versus the Eulerian strain measure ($f = 0.5[(V_0/V)^{2/3} - 1]$). The solid curve is the fitted isotherm of the cubic phase, with the dashed curves indicating 1σ uncertainty. (b) $(Mg_{0.8}Fe_{0.2})O$ high-spin data fitted in the region 0 – 40 GPa with the Birch–Murnaghan equation of state

Figure 4. Isothermal compression curves of $(Mg_{1-x}Fe_x)O$ (x = 0.17-0.2), based on the combined datasets from the present study and from Lin et al. [2005]. The black curve is the isotherm for the high-spin state, as determined by fitting the data between 0 and 40 GPa with the Birch–Murnaghan equation (shown in the inset). The grey curve is the MgO isotherm after Speziale et al. [2001]. The same data shown as normalized pressure versus Eulerian strain (*inset*) yield the solid curve as the best-fit isotherm for the high-spin phase, and the dashed curves represent 1σ uncertainties.

Figure 5. Static-compression results for $(Mg_{1-x}Fe_x)O$ (x = 0.17-0.2) plotted in terms of normalized pressure *G* versus Eulerian strain referred to the starting volume of the high-spin phase, *g* (see text). Data between 40 and 80 GPa are interpreted as coexisting high-spin and low-spin phases, whereas data above 80 GPa are assigned to the low-spin state. The solid black line is the isotherm for the high-spin phase determined by fitting the data below 40 GPa with the Birch–Murnaghan equation of state. The dashed line is the isotherm for the low-spin phase, and the dotted curve is the MgO isotherm of Speziale et al. [2001] with the grey area indicating its 1σ uncertainty. The inset shows the deviation of the experimental data from the isotherm for the high-spin phase (solid squares), with the dashed grey line giving the deviation of the MgO isotherm.

Figure 6. Relative difference of unit-cell volume and bulk sound velocity between the low-spin phase of $(Mg_{1-x}Fe_x)O$ (x = 0.17-0.2) and pure MgO.

Figure 7. Third order Birch–Murnaghan isotherms for the high-spin (squares) and low-spin (circles) phases of $(Mg_{1-x}Fe_x)O$ (x = 0.17-0.2) plotted in terms of normalized pressure *F* versus Eulerian strain *f*. The different models are characterized by different starting volumes for the low-spin state, expressed as the ratio V_0^{LS}/V_0^{HS}. The inset summarizes the same information plotted as volume versus pressure. See Table 4 for fit parameters.

Figure 8. Trade-off between goodness of fit (expressed as χ^2) and data misfit (expressed as root mean square difference between data and model pressure) for the different model isotherms of the low-spin phase of $(Mg_{1-x}Fe_x)O$ (x = 0.17-0.2) (see text for explanations) shown in Fig. 6 (see text for explanations). For comparison, average experimental uncertainties are shown as a grey shaded area in the inset.

Figure 9. Calculated percentage differences in unit-cell volume (a), bulk modulus (b) and bulk sound velocity (c) between the the high- and low-spin forms of $(Mg_{1-x}Fe_x)O$ (x = 0.17-0.2) at pressures between 40 and 80 GPa. The different curves show results for starting-volume ratios V_0^{LS}/V_0^{HS} ranging between 0.88 and 1.0 at fixed intervals of 0.01 V_0^{LS}/V_0^{HS}.

Figure 10. Models of the pressure dependence of the abundance of low-spin relative to high-spin states, compared with experimental results obtained by Mössbauer spectroscopy [Speziale et al., 2005]. The solid black curve indicates the model discussed in the text.

Figure 11. Summary of the calculated relative unit-cell volume decrease and bulk sound velocity increase normalized by the molar fraction of low-spin phase, shown as a function of pressure. (a) Unit-cell volume change in the case of progressive spin transition between 40 and 80 GPa; (b) velocity change for the same model. (c) Unit-cell volume variation in the case of progressive spin transition between 30 and 120 GPa; (d) velocity change for the same model. The central curves correspond to $V_0^{LS}/V_0^{HS} = 0.94$, our preferred model, and the shaded area represents the range of models computed for V_0^{LS}/V_0^{HS} ranging between 0.88 and 1.0.

Figure 12. Summary of (a) the modeled unit-cell volume decrease and (b) bulk sound velocity increase for the cases of complete high- to low-spin transition at 40 GPa (open squares) and at 80 GPa (open circles), and for the cases of progressive transition between 40 and 80 GPa (filled circles) and between 30 and 120 GPa (filled triangles). The results are plotted as a function of assumed zero-pressure volume for the low-spin phase, with $V_0^{LS}/V_0^{HS} = 0.94$ being our preferred model.

Figure 13. Relative density and bulk modulus disagreement between a pyrolitic mineralogical model and the PREM seismological model (see text for details). The three sets of curves represent: model with no spin transition in magnesiowüstite, a model with progressive spin transition across the pressure range 40 – 80 GPa and a model with spin transition across the range between 30 and 120 GPa. The large error bars under the legend correspond to 1σ when considering only the uncertainties in the thermal parameters θ_0, γ_0 and q for the three mineral phases in the models. The error bars along the curves reflect the uncertainties in the 300 K isotherms of the mineral phases of the models, so show how well resolved the systematic effects of the spin transition may be (assuming no compensating effects due to changes in thermal properties across the spin transition).

Figure 14. Relative density and bulk modulus disagreement between a pyrolitic mineralogical model and the PREM seismological model, shown as a function of temperature and including the effect of spin transition of Fe^{2+} in magnesiowüstite (see text for details). Cases are shown for a progressive spin transition across the pressure range 40-80 GPa (a) and 30-20 GPa (b), with error bars as in Fig. 13.

Figure 15. Relative density and bulk modulus disagreement with respect to PREM of a pyrolite-like mineralogical model with progressive spin transition in magnesiowüstite between 30 and 120 GPa. The effect of increasing the amount of magnesiowüstite from 31 to 40 mol percent, both along a geotherm and along a 2800 K isotherm, is shown, along with a model with 31 mol percent magnesiowüstite (standard pyrolite of Lee et al. [2004]) along a geotherm *P*-*T* path.

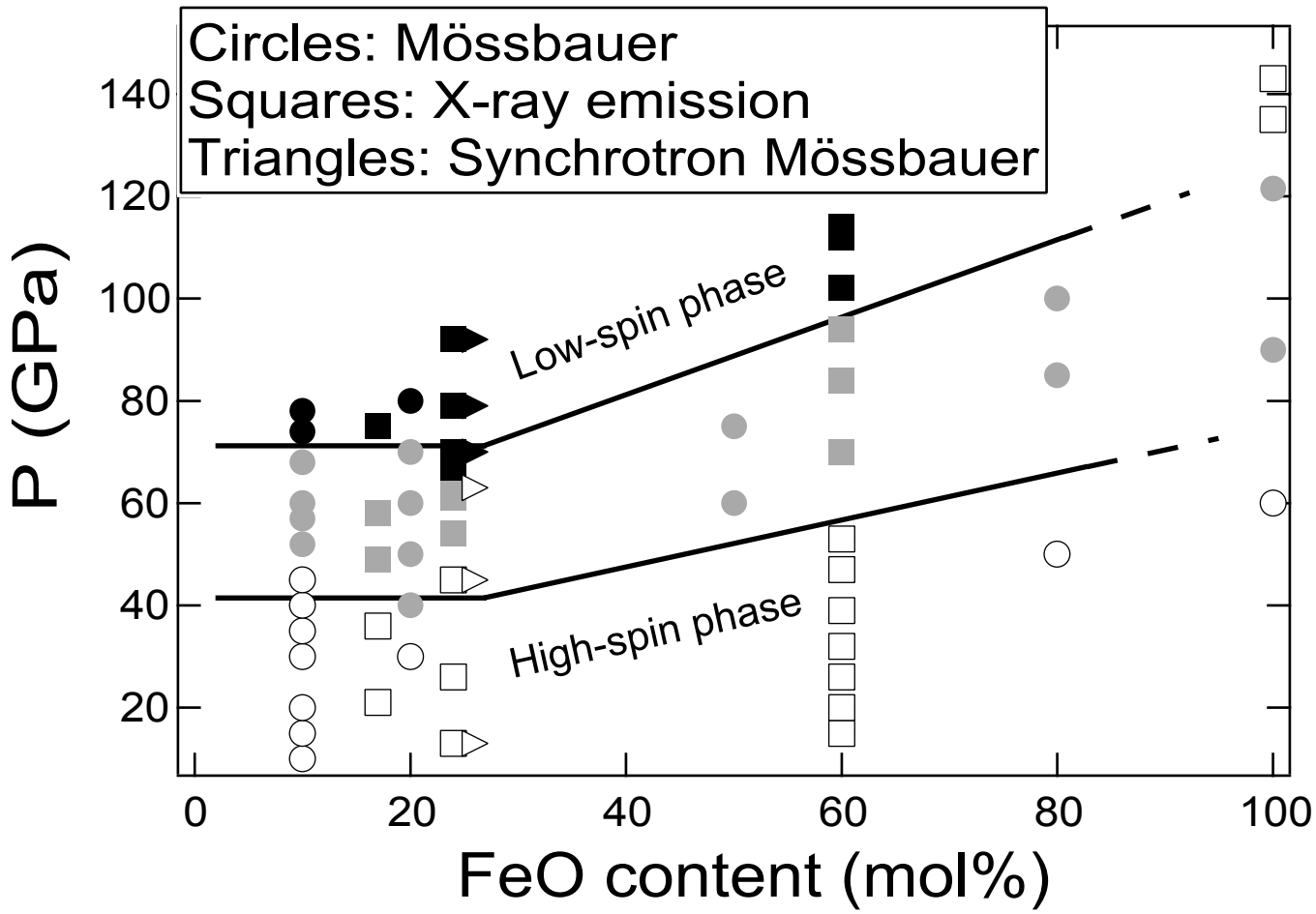
Circles: Mössbauer
Squares: X-ray emission
Triangles: Synchrotron Mössbauer
Low-spin phase
High-spin phase
P (GPa)
FeO content (mol%)
140
120
100
80
60
40
20
0
20
40
60
80
100

Figure 1

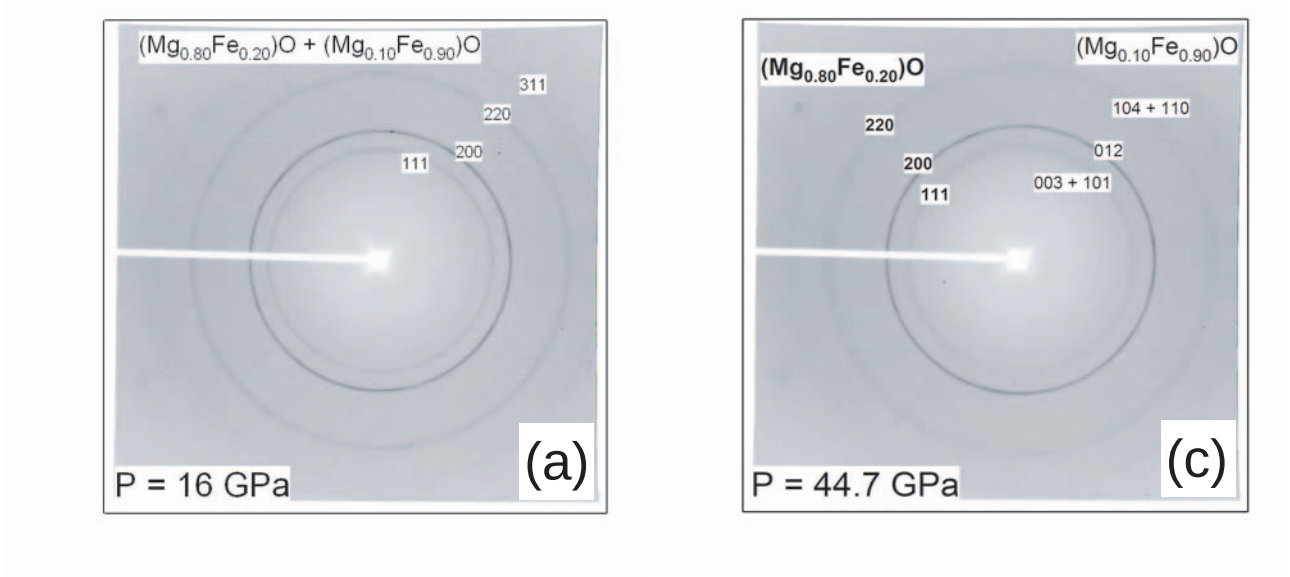
(Mg0.80Fe0.20)O + (Mg0.10Fe0.90)O
311
220
200
111
P = 16 GPa
(a)
(Mg0.80Fe0.20)O
(Mg0.10Fe0.90)O
104 + 110
220
012
200
003 + 101
111
P = 44.7 GPa
(c)

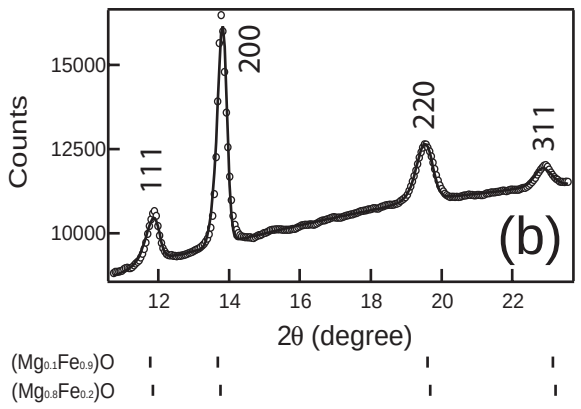
Counts
15000
12500
10000
111
200
220
311
(b)
12
14
16
18
20
22
2θ (degree)
(Mg0.1Fe0.9)O
(Mg0.8Fe0.2)O

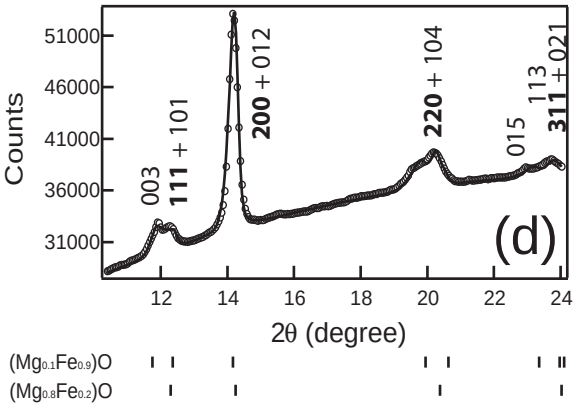
Counts
51000
46000
41000
36000
31000
003
111 + 101
200 + 012
220 + 104
015
113
311 + 021
(d)
12
14
16
18
20
22
24
2θ (degree)
(Mg0.1Fe0.9)O
(Mg0.8Fe0.2)O

Figure 2

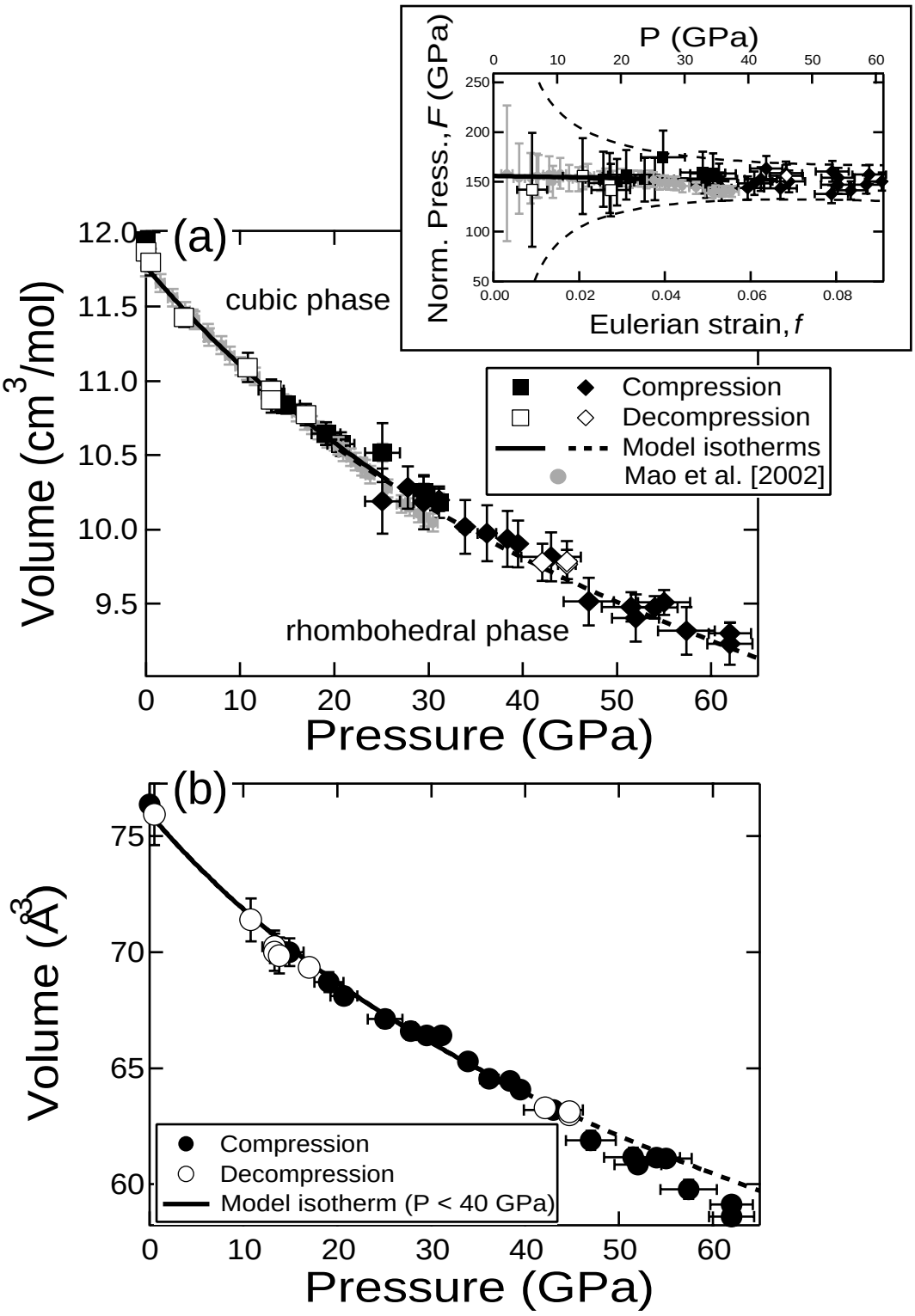
(a)
cubic phase
rhombohedral phase
Volume (cm3/mol)
Pressure (GPa)
Compression
Decompression
Model isotherms
Mao et al. [2002]
P (GPa)
Norm. Press., F (GPa)
Eulerian strain, f
(b)
Volume (Å3)
Pressure (GPa)
Compression
Decompression
Model isotherm (P < 40 GPa)

Figure 3

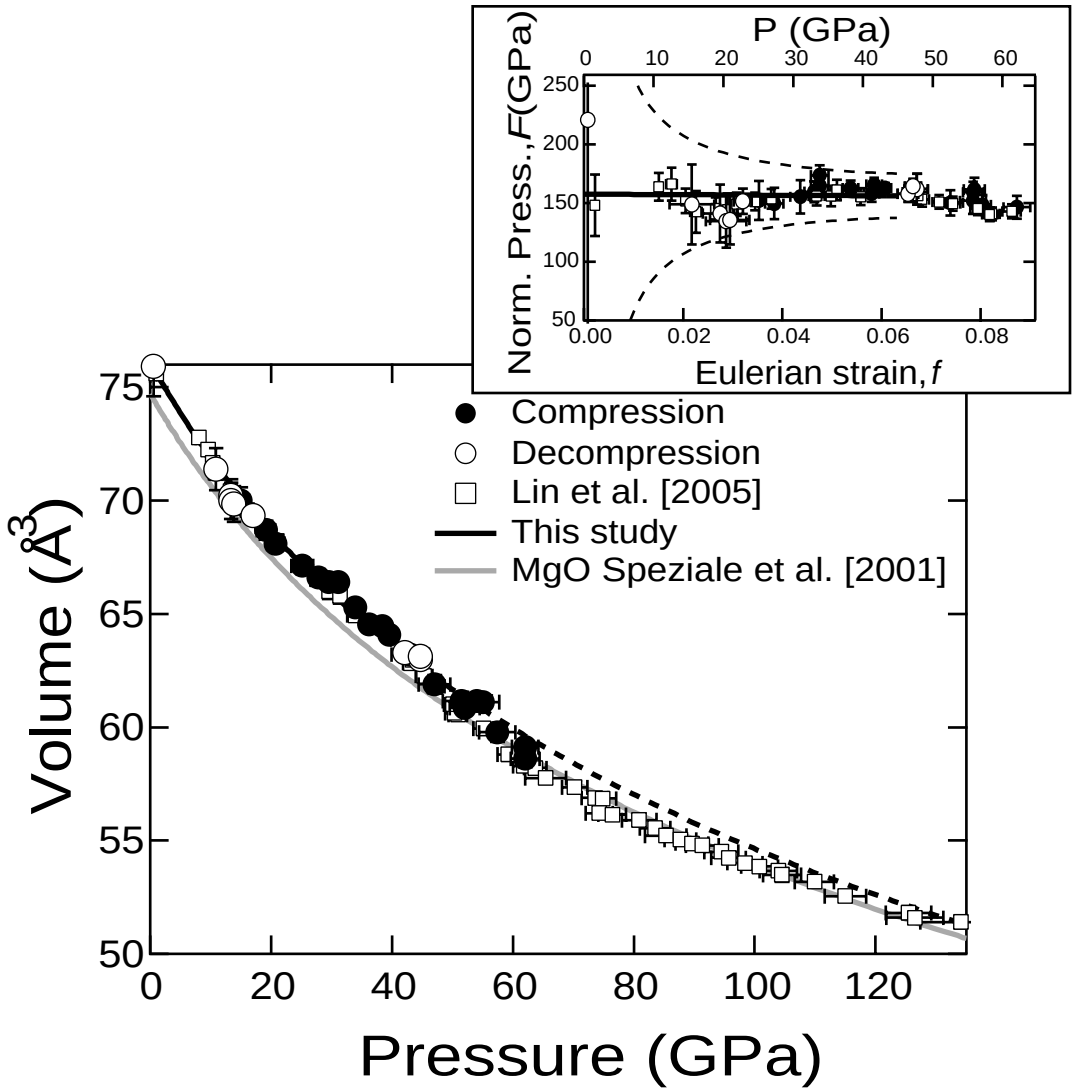
P (GPa)
0
10
20
30
40
50
60
Norm. Press., F(GPa)
250
200
150
100
50
0.00
0.02
0.04
0.06
0.08
Eulerian strain, f
Compression
Decompression
Lin et al. [2005]
This study
MgO Speziale et al. [2001]
Volume (Å3)
75
70
65
60
55
50
0
20
40
60
80
100
120
Pressure (GPa)

Figure 4

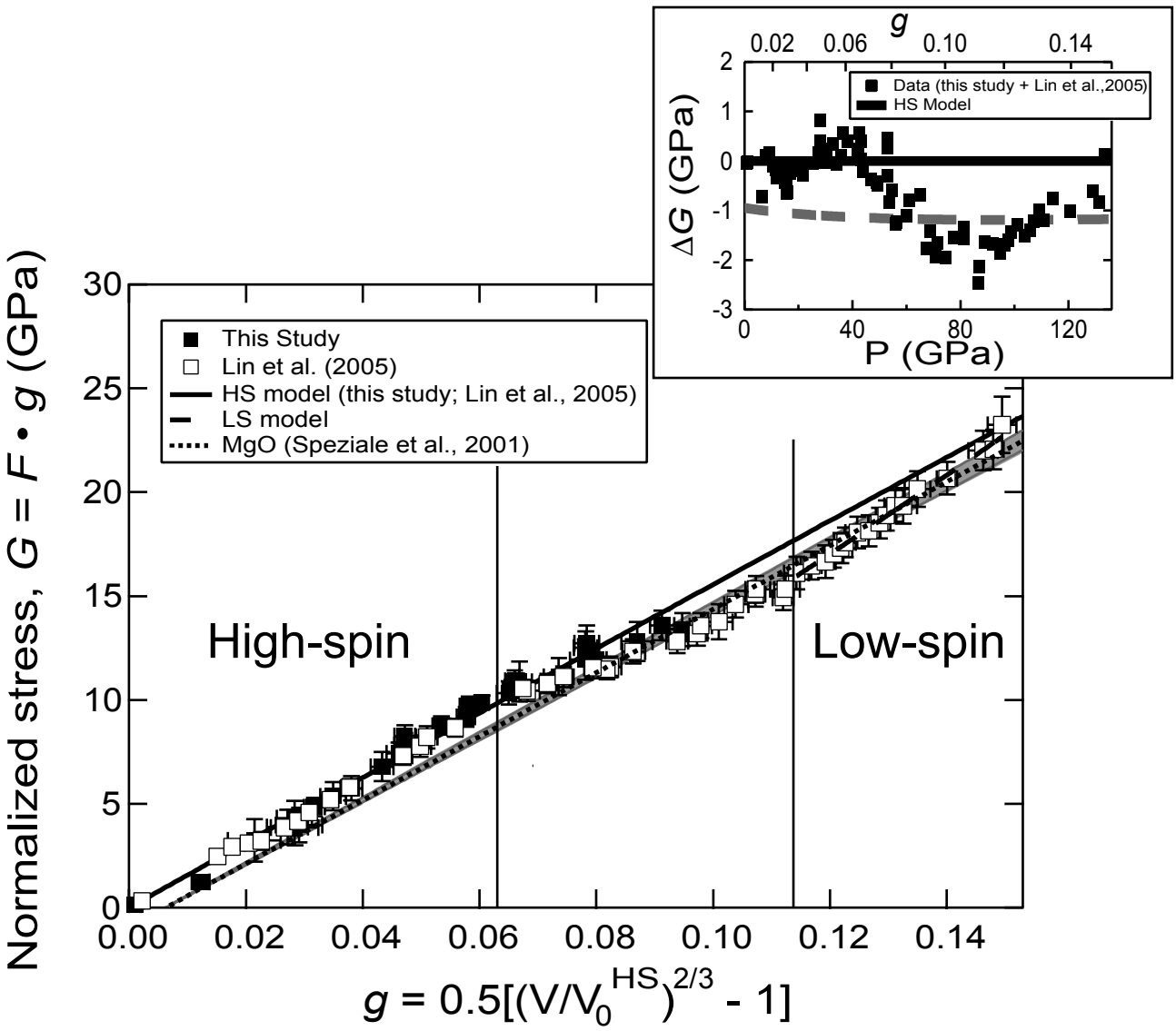
Normalized stress, $G = F \bullet g$ (GPa)
$g = 0.5[(V/V_0^{HS})^{2/3} - 1]$
This Study
Lin et al. (2005)
HS model (this study; Lin et al., 2005)
LS model
MgO (Speziale et al., 2001)
High-spin
Low-spin
0.00
0.02
0.04
0.06
0.08
0.10
0.12
0.14
0
5
10
15
20
25
30
g
0.02
0.06
0.10
0.14
ΔG (GPa)
P (GPa)
Data (this study + Lin et al.,2005)
HS Model
2
1
0
-1
-2
-3
0
40
80
120

Figure 5

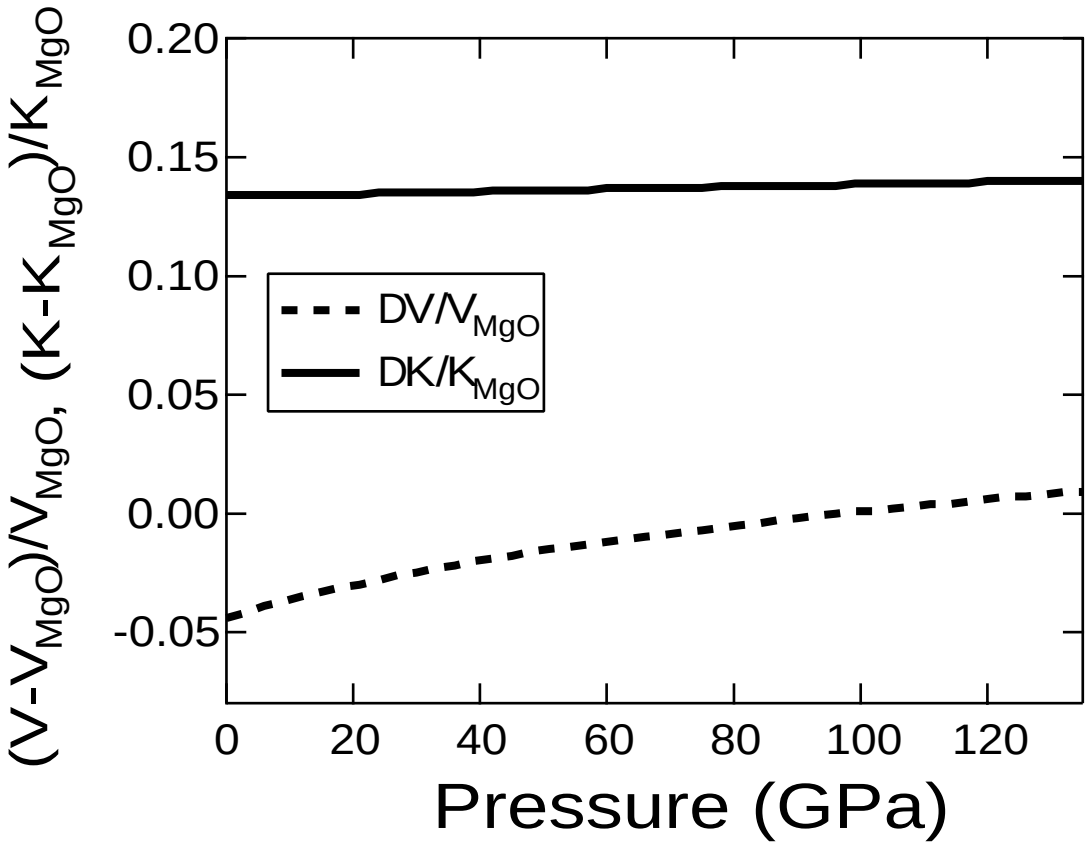
0.20
0.15
0.10
0.05
0.00
-0.05
0
20
40
60
80
100
120
Pressure (GPa)
(V-V_MgO)/V_MgO, (K-K_MgO)/K_MgO
DV/V_MgO
DK/K_MgO

Figure 6

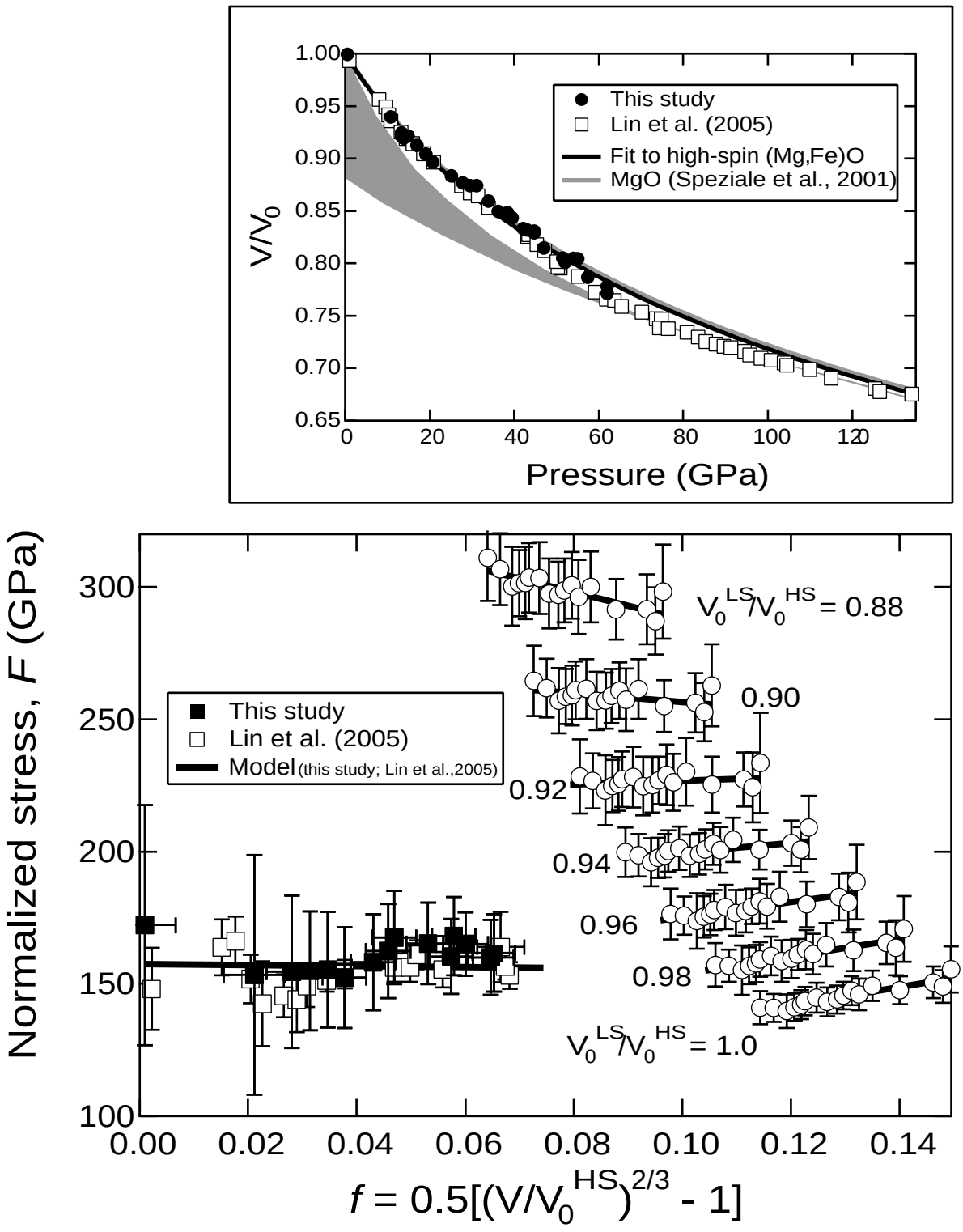
1.00
0.95
0.90
0.85
0.80
0.75
0.70
0.65
V/V0
0
20
40
60
80
100
120
Pressure (GPa)
This study
Lin et al. (2005)
Fit to high-spin (Mg,Fe)O
MgO (Speziale et al., 2001)
300
250
200
150
100
Normalized stress, F (GPa)
0.00
0.02
0.04
0.06
0.08
0.10
0.12
0.14
f = 0.5[(V/V0HS)2/3 - 1]
This study
Lin et al. (2005)
Model (this study; Lin et al.,2005)
V0LS/V0HS = 0.88
0.90
0.92
0.94
0.96
0.98
V0LS/V0HS = 1.0

Figure 7

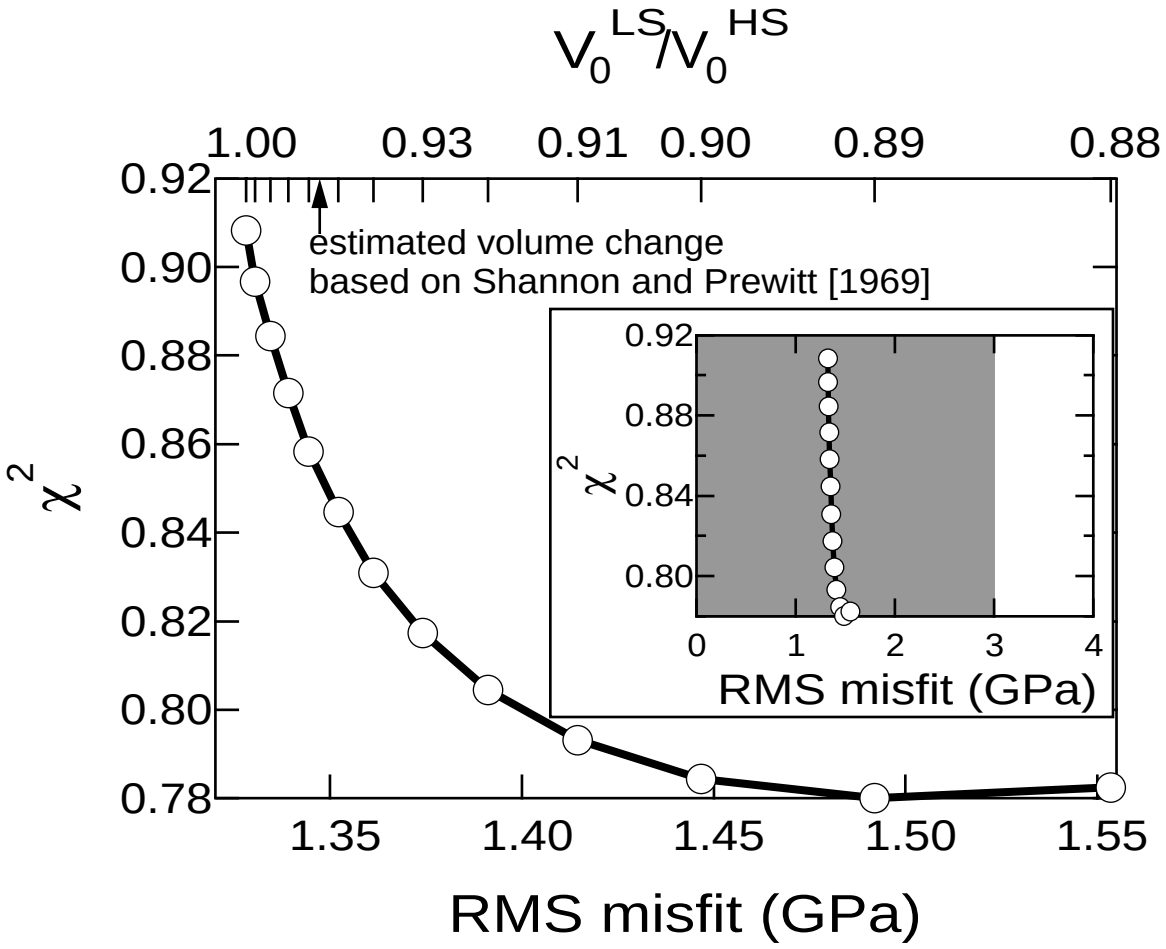
V_0^{LS}/V_0^{HS}
1.00
0.93
0.91
0.90
0.89
0.88
0.92
0.90
0.88
0.86
0.84
0.82
0.80
0.78
χ^2
estimated volume change
based on Shannon and Prewitt [1969]
0.92
0.88
0.84
0.80
χ^2
0
1
2
3
4
RMS misfit (GPa)
1.35
1.40
1.45
1.50
1.55
RMS misfit (GPa)

Figure 8

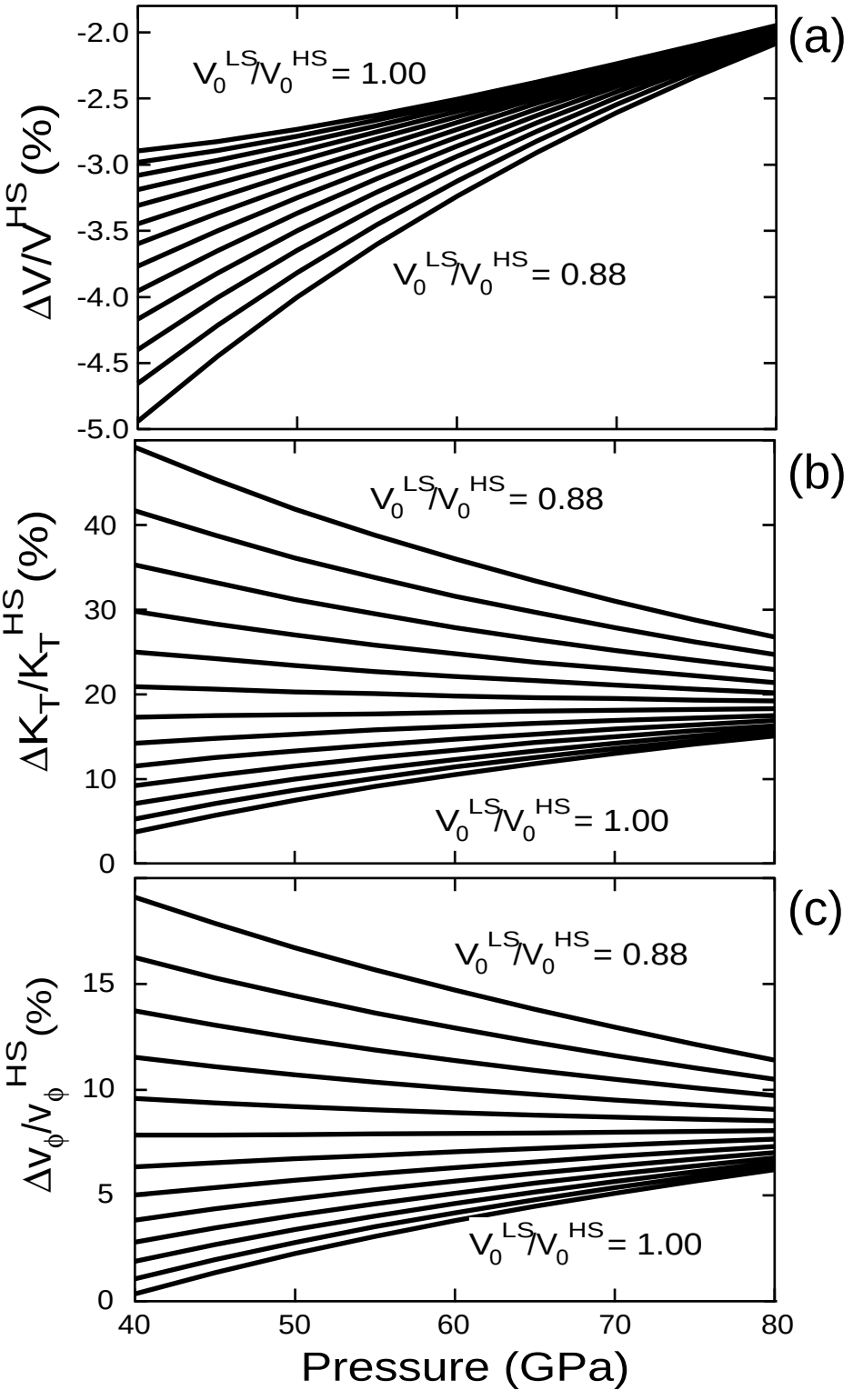
(a)
V_0^{LS}/V_0^{HS} = 1.00
V_0^{LS}/V_0^{HS} = 0.88
$\Delta V/V^{HS}$ (%)
-2.0
-2.5
-3.0
-3.5
-4.0
-4.5
-5.0
(b)
V_0^{LS}/V_0^{HS} = 0.88
V_0^{LS}/V_0^{HS} = 1.00
$\Delta K_T/K_T^{HS}$ (%)
40
30
20
10
0
(c)
V_0^{LS}/V_0^{HS} = 0.88
V_0^{LS}/V_0^{HS} = 1.00
$\Delta v_\phi/v_\phi^{HS}$ (%)
15
10
5
0
40
50
60
70
80
Pressure (GPa)

Figure 9

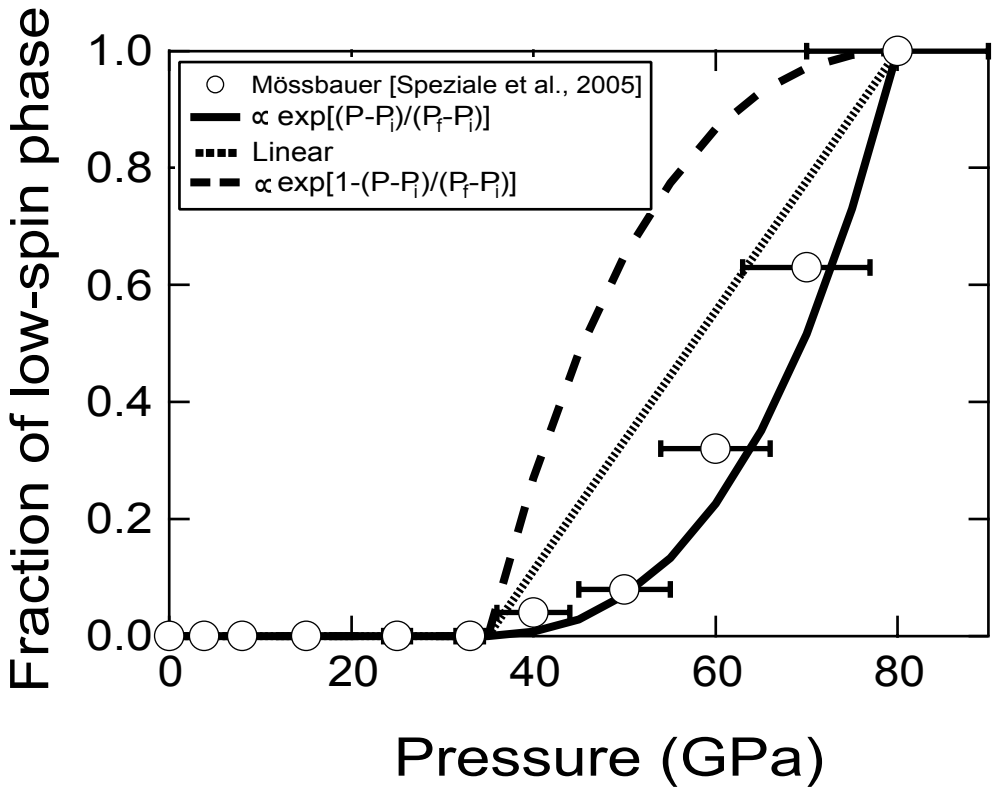
Fraction of low-spin phase
1.0
0.8
0.6
0.4
0.2
0.0
0
20
40
60
80
Pressure (GPa)
Mössbauer [Speziale et al., 2005]
∝ exp[(P-P$_i$)/(P$_f$-P$_i$)]
Linear
∝ exp[1-(P-P$_i$)/(P$_f$-P$_i$)]

Figure 10

Figure 11

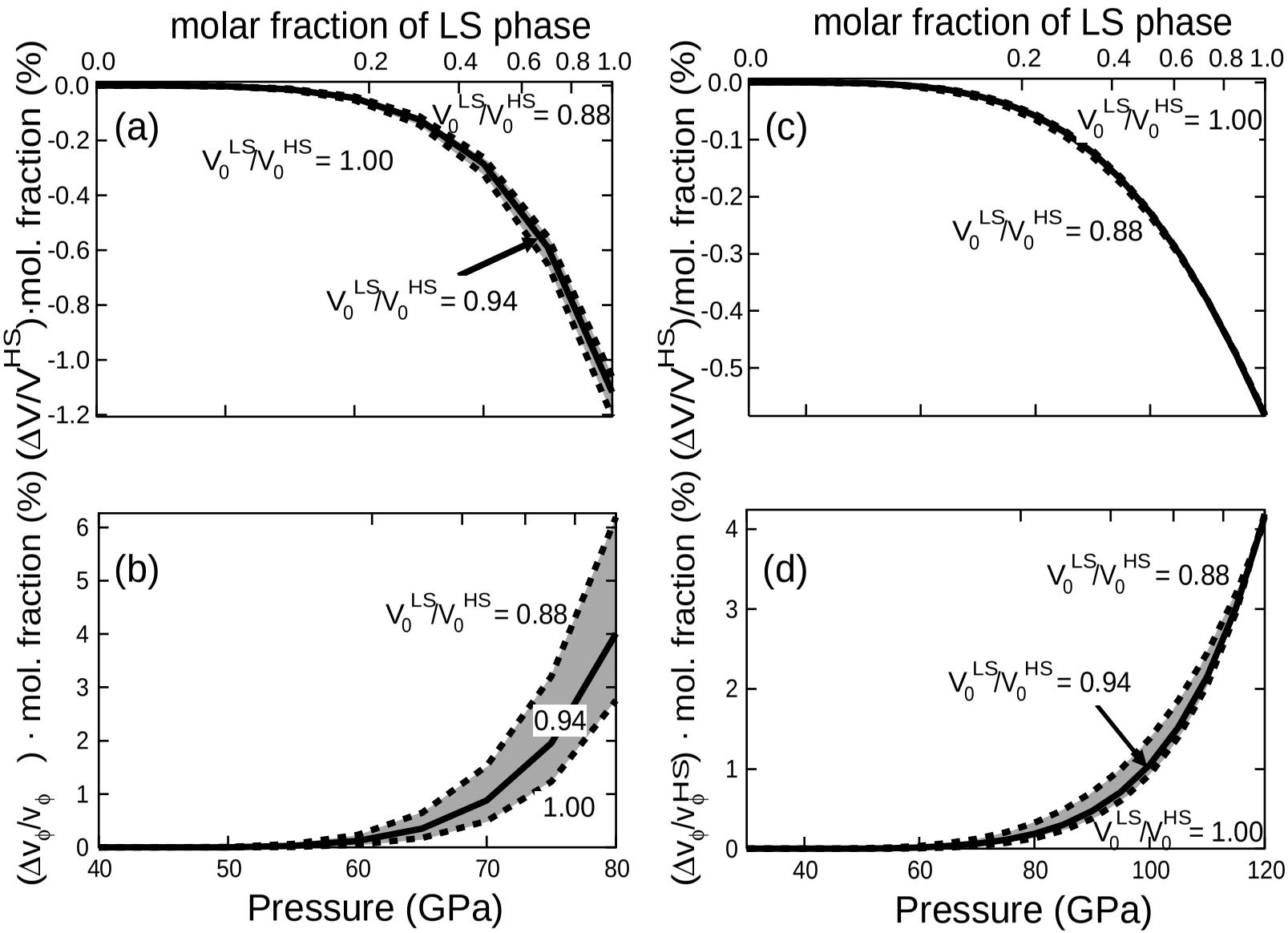
molar fraction of LS phase
(a)
V_0^{LS}/V_0^{HS} = 0.88
V_0^{LS}/V_0^{HS} = 1.00
V_0^{LS}/V_0^{HS} = 0.94
$(\Delta V/V^{HS})$·mol. fraction (%)
(b)
V_0^{LS}/V_0^{HS} = 0.88
0.94
1.00
$(\Delta v_\phi/v_\phi)$ · mol. fraction (%)
Pressure (GPa)
molar fraction of LS phase
(c)
V_0^{LS}/V_0^{HS} = 1.00
V_0^{LS}/V_0^{HS} = 0.88
$(\Delta V/V^{HS})$/mol. fraction (%)
(d)
V_0^{LS}/V_0^{HS} = 0.88
V_0^{LS}/V_0^{HS} = 0.94
V_0^{LS}/V_0^{HS} = 1.00
$(\Delta v_\phi/v_\phi^{HS})$ · mol. fraction (%)
Pressure (GPa)

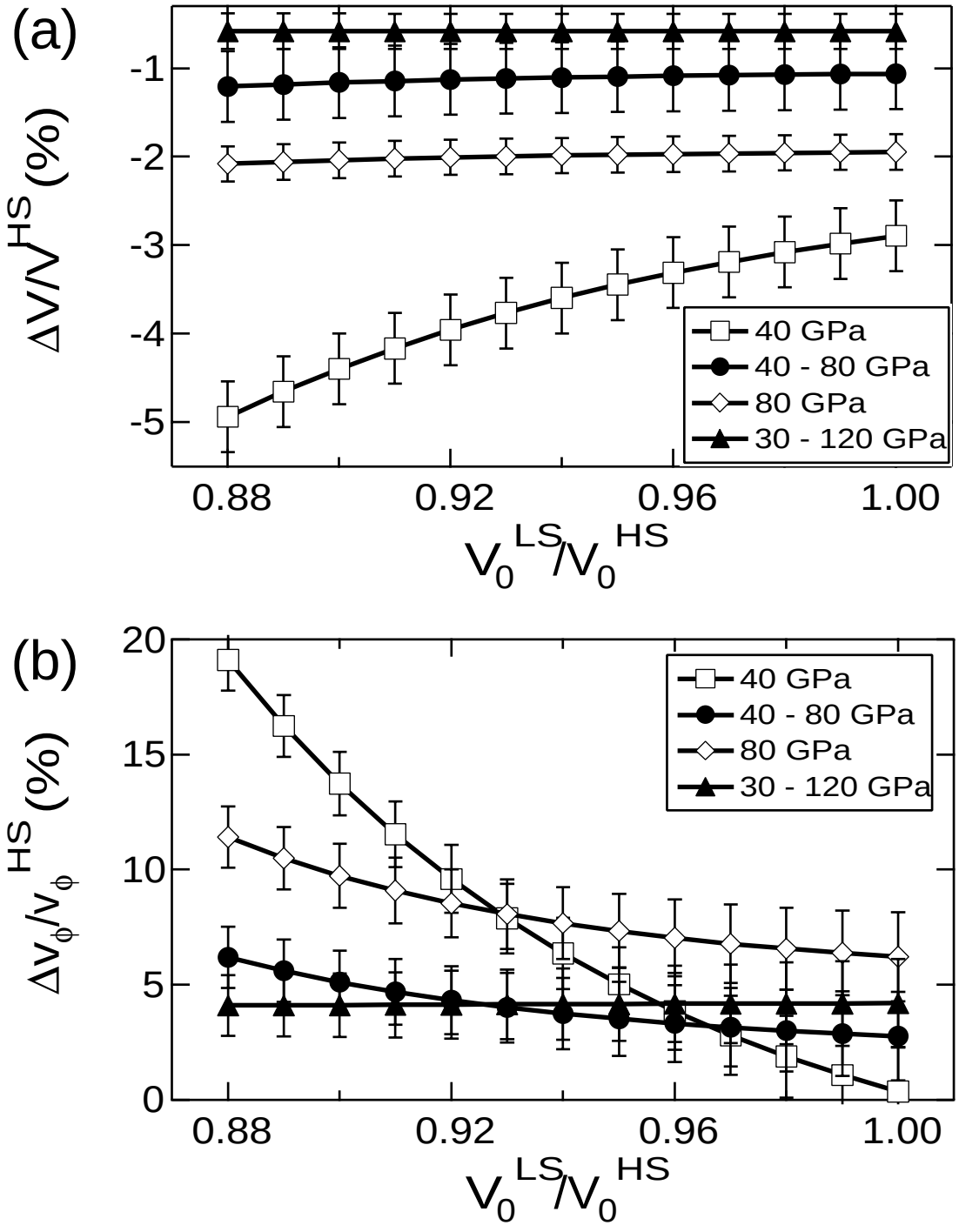
(a)
$\Delta V/V^{HS}$ (%)
-1
-2
-3
-4
-5
0.88
0.92
0.96
1.00
V_0^{LS}/V_0^{HS}
40 GPa
40 - 80 GPa
80 GPa
30 - 120 GPa
(b)
$\Delta v_\phi/v_\phi^{HS}$ (%)
20
15
10
5
0
0.88
0.92
0.96
1.00
V_0^{LS}/V_0^{HS}
40 GPa
40 - 80 GPa
80 GPa
30 - 120 GPa

Figure 12

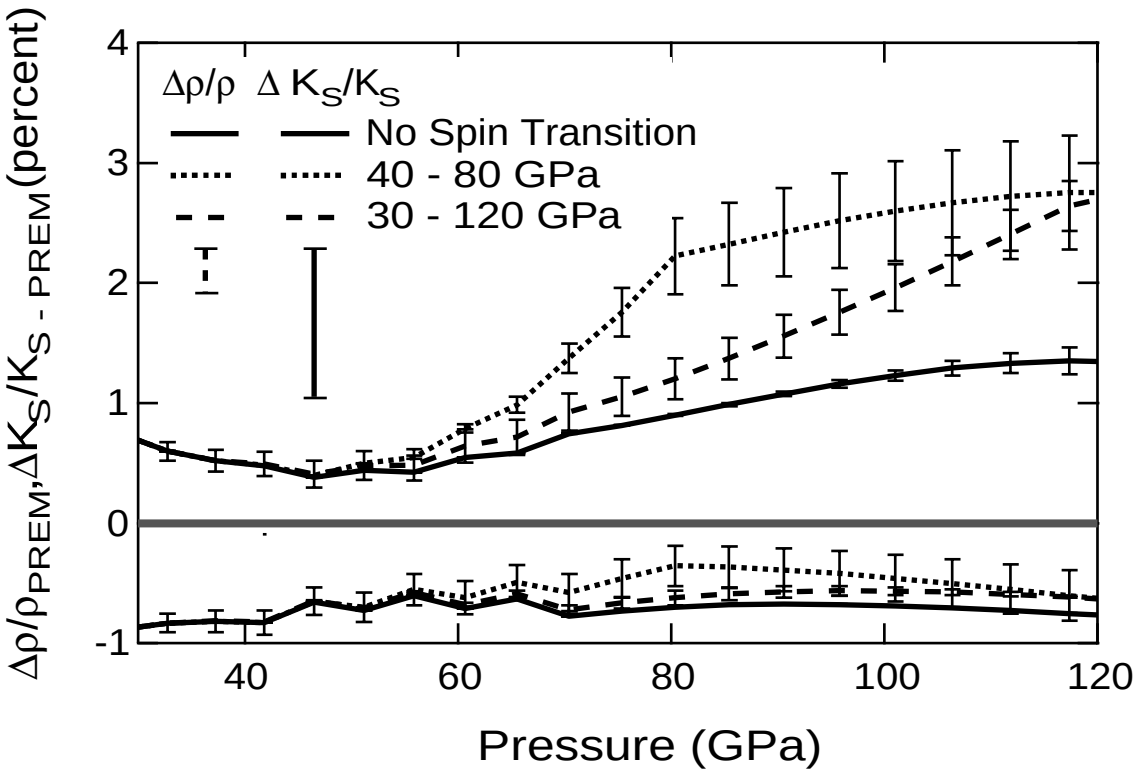
Δρ/ρ Δ K_S/K_S
No Spin Transition
40 - 80 GPa
30 - 120 GPa
Δρ/ρ_PREM,ΔK_S/K_S - PREM(percent)
Pressure (GPa)
4
3
2
1
0
-1
40
60
80
100
120

Figure 13

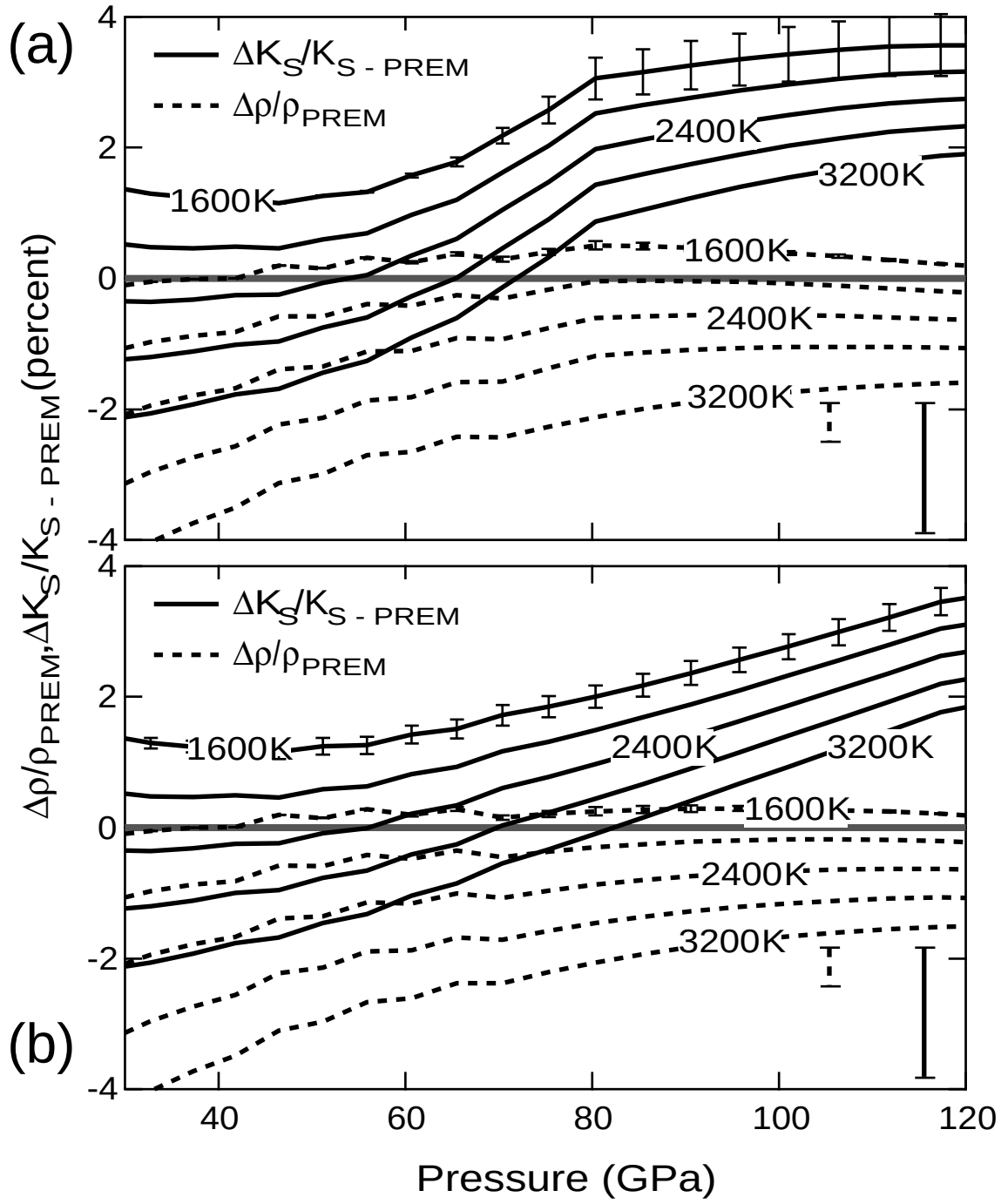
(a)
(b)
$\Delta K_S/K_{S\text{ - PREM}}$
$\Delta\rho/\rho_{PREM}$
1600K
2400K
3200K
$\Delta\rho/\rho_{PREM}$,$\Delta K_S/K_{S\text{ - PREM}}$(percent)
Pressure (GPa)
4
2
0
-2
-4
40
60
80
100
120

Figure 14

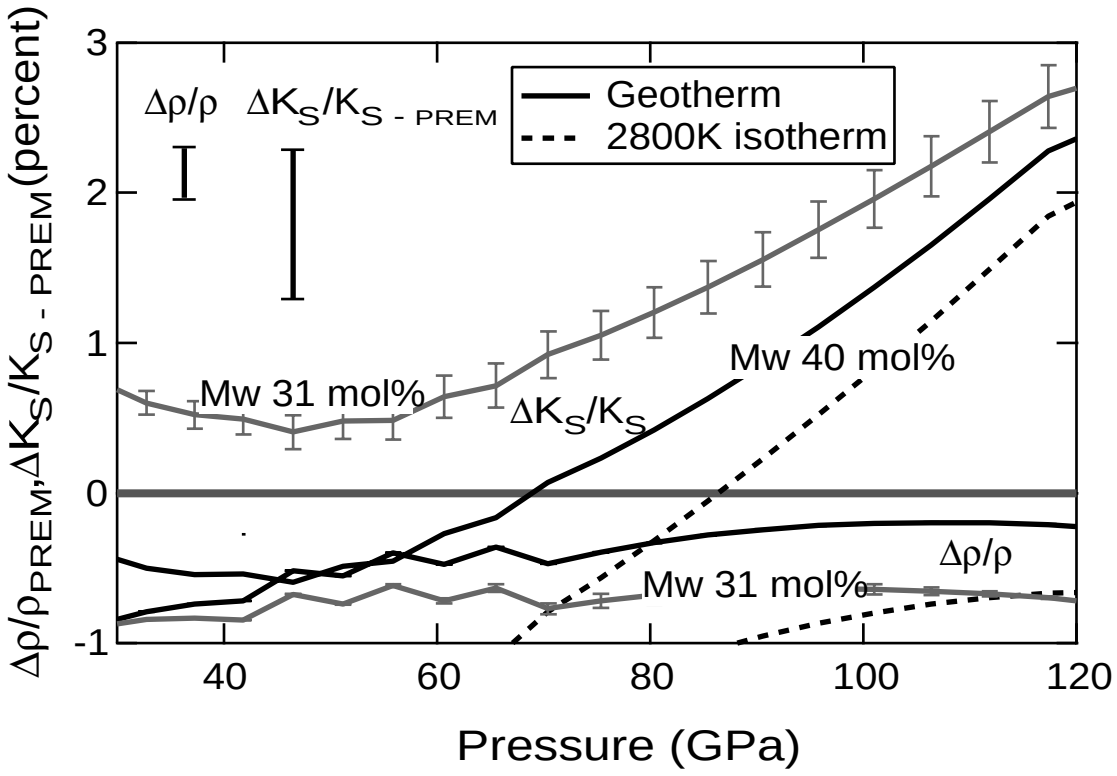
Δρ/ρ
ΔK_S/K_S - PREM
Geotherm
2800K isotherm
Mw 31 mol%
ΔK_S/K_S
Mw 40 mol%
Δρ/ρ
Mw 31 mol%
Δρ/ρ_PREM, ΔK_S/K_S - PREM (percent)
Pressure (GPa)
3
2
1
0
-1
40
60
80
100
120

Figure 15